2015

Vibrational Spectroscopy of Photosystem I

Gary Hastings
Georgia State University, ghastings@gsu.edu

Recommended Citation

Hastings, Gary. 2015. "Vibrational Spectroscopy of Photosystem I." Biochimica et Biophysica Acta (BBA) - Bioenergetics, Vibrational spectroscopies and bioenergetic systems, 1847 (1): 55–68. doi:10.1016/j.bbabio.2014.07.014.

Biochimica et Biophysica Acta 1847 (2015) 55–68

Contents lists available at ScienceDirect

Biochimica et Biophysica Acta

journal homepage: www.elsevier.com/locate/bbabio

Review

Vibrational spectroscopy of photosystem I☆

Gary Hastings

Department of Physics and Astronomy, Georgia State University, Atlanta, GA 30303, USA

ARTICLE INFO

Article history:
Received 29 April 2014
Received in revised form 1 July 2014
Accepted 21 July 2014
Available online 30 July 2014

Keywords:
Photosynthesis
Photosystem I
FTIR
Time-resolved step-scan
A_1
Normal mode

ABSTRACT

Fourier transform infrared difference spectroscopy (FTIR DS) has been widely used to study the structural details of electron transfer cofactors (and their binding sites) in many types of photosynthetic protein complexes. This review focuses in particular on work that has been done to investigate the A_1 cofactor in photosystem I photosynthetic reaction centers. A review of this subject area last appeared in 2006 [1], so only work undertaken since then will be covered here.

Following light excitation of intact photosystem I particles the $P700^+A_1^-$ secondary radical pair state is formed within 100 ps. This state decays within 300 ns at room temperature, or 300 μs at 77 K. Given the short-lived nature of this state, it is not easily studied using "static" photo-accumulation FTIR difference techniques at either temperature. Time-resolved techniques are required. This article focuses on the use of time-resolved step-scan FTIR DS for the study of the $P700^+A_1^-$ state in intact photosystem I. Up until now, only our group has undertaken studies in this area. So, in this article, recent work undertaken in our lab is described, where we have used low-temperature (77 K), microsecond time-resolved step-scan FTIR DS to study the $P700^+A_1^-$ state in photosystem I. In photosystem I a phylloquinone molecule occupies the A_1 binding site. However, different quinones can be incorporated into the A_1 binding site, and here work is described for photosystem I particles with plastoquinone-9, 2-phytyl naphthoquinone and 2-methyl naphthoquinone incorporated into the A_1 binding site. Studies in which ^{18}O isotope labeled phylloquinone has been incorporated into the A_1 binding site are also discussed.

To fully characterize PSI particles with different quinones incorporated into the A_1 binding site nanosecond to millisecond visible absorption spectroscopy has been shown to be of considerable value, especially so when undertaken using identical samples under identical conditions to that used in time-resolved step-scan FTIR measurements. In this article the latest work that has been undertaken using both visible and infrared time resolved spectroscopies on the same sample will be described.

Finally, vibrational spectroscopic data that has been obtained for phylloquinone in the A_1 binding site in photosystem I is compared to corresponding data for ubiquinone in the Q_A binding site in purple bacterial reaction centers. This article is part of a Special Issue entitled: Vibrational spectroscopies and bioenergetic systems.

1. Overview

This review focusses on the use of low-temperature (77 K), microsecond time-resolved step-scan (TRSS) FTIR difference spectroscopy (DS) to study the quinones occupying the A_1 binding site in photosystem I (PSI) photosynthetic reaction centers (RC). In Section 2 the role PSI plays in photosynthesis is described, and the cofactors involved in light-driven electron transfer leading to solar energy conversion are introduced. The energetics of the solar conversion process in PSI is outlined, and specific structural details of the quinone cofactor occupying the A_1 protein binding site are introduced. Other quinones that have been incorporated into the A_1 binding site and studied using TRSS FTIR DS are discussed. In Section 3 TRSS FTIR DS is presented and early work that was undertaken to assign the bands in the spectra is outlined. Computational work that has been undertaken to help assess the appropriateness of proposed band assignments is reviewed. In Section 4 recent works undertaken using PSI particles with isotope labeled quinone incorporated, or completely different quinones incorporated, are discussed. In Section 5 vibrational spectroscopy studies associated with quinones in the Q_A binding site in purple bacterial reaction centers are briefly outlined and compared to vibrational spectroscopy studies associated with quinones in the A_1 binding site.

Abbreviations: A_1, secondary electron acceptor bound in photosystem I; Chl-a, chlorophyll-*a*; DFT, density functional theory; DS, difference spectra/spectrum/spectroscopy/spectroscopic; DDS, double difference spectrum; C═O, carbonyl; ET, electron transfer; FTIR, Fourier transform infrared; H-bond, hydrogen bond; μs, microsecond; ms, millisecond; MM, molecular mechanics; ns, nanosecond; NQ, 1,4-naphthoquinone; OD, optical density; PSI, photosystem one; PQ_9, plastoquinone-9; PhQ, phylloquinone (2-methyl, 3-phytyl 1,4-naphthoqiuinone); PBRC, purple bacterial reaction center; QM, quantum mechanical; RC, reaction center; *Rb*, *Rhodobacter*; RT, room temperature; *S6803*, *Synechocystis* sp. PCC 6803; TR, time-resolved; WT, wild type, 2MNQ, 2-methyl, 1,4-naphthoquinone; 2PhNQ, 2-phytyl 1,4-naphthoquinone

☆ This article is part of a Special Issue entitled: Vibrational spectroscopies and bioenergetic systems.

http://dx.doi.org/10.1016/j.bbabio.2014.07.014
0005-2728/

2. Introduction

In photosynthesis, light drives a set of reactions that result in products essential for the maintenance of life on earth [2]. In oxygen evolving organisms two photosystems, called photosystems one and two (PSI and PSII), capture and convert solar energy independently [2–4]. The solar conversion reactions occur in a centralized pigment-protein unit called a reaction center (RC). In the RC, light is used to drive electrons vectorially, via a series of acceptors, across a biological membrane. This separation of charges over a biological membrane is the principle mechanism of solar energy conversion in all photosynthetic systems.

From a global perspective, PSI catalyzes the formation of the reducing product NADPH that is used to assimilate carbon dioxide into complex organic molecules [2]. More specifically, PSI is the enzyme that uses light to catalyze the transfer of electrons from plastocyanin to ferredoxin across the thylakoid membrane [5]. PSI consists of 13 or more protein subunits, many of which have been characterized [6–9]. The electron transfer (ET) cofactors are bound to the membrane-spanning protein subunits called PsaA and PsaB [10]. The terminal ET components, F_A and F_B, are bound to the PsaC subunit. The arrangement of the ET cofactors in the PSI RC is outlined in Fig. 1. The cofactors bound to PsaA or PsaB are labeled with a subscript A or B, respectively. Fig. 1 is generated using the 2.5 Å x-ray crystal structure of trimeric PSI particles from the cyanobacterium *Synechococcus elongatus* (PDB file accession number 1JB0) [10].

P700, the primary electron donor in PSI, is a dimeric chlorophyll-a (Chl-*a*) species [11]. Actually P700 is a Chl-a/Chl-a′ heterodimeric species (P_B/P_A in Fig. 1), were Chl-a′ is an epimer of Chl-a [12]. The primary electron acceptor, A_0, is a monomeric Chl-*a* molecule [13]. A_1 is a phylloquinone (PhQ) molecule [9]. PhQ (or vitamin K_1) is a 2-methyl, 3-phytyl, 1, 4-naphthaquinone, the structure of which is shown in Fig. 3. F_X, F_A and F_B are (4Fe-4S) iron sulfur clusters [14,15].

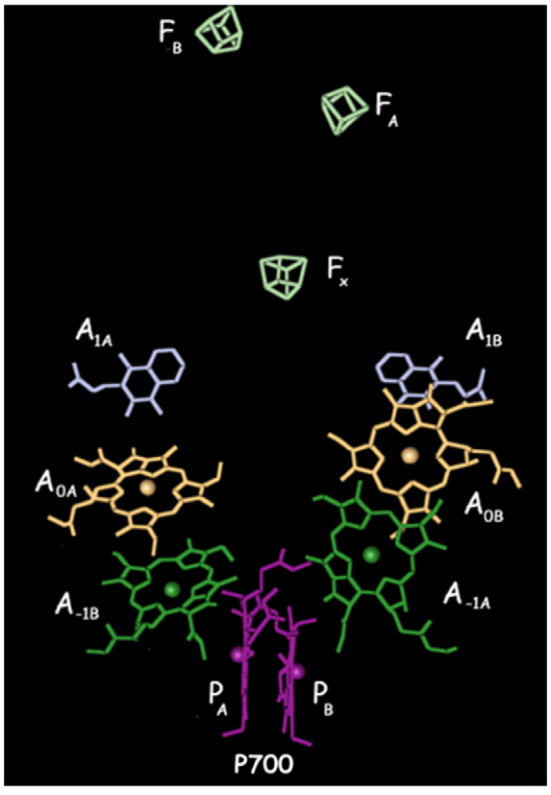

Fig. 1. Arrangement of the two branches of ET cofactors in PSI. Number subscript refers to cofactor. Letter subscript refers to protein subunit (PsaA or B) to which cofactor is bound. F_A and F_B are bound to the PsaC subunit.

In PSI, following light excitation of P700, an electron is transferred to A_0, in <5 ps (Fig. 2) [16]. Stabilization of the charge-separated state is achieved by ET from A_0^- to A_1 in <50 ps [16,17]. To further stabilize the charge separated state, the electron is transferred from A_1^- to F_X in ~280 ns at room temperature (RT) [18], and then on to F_A and F_B (Fig. 2).

In cyanobacterial PSI particles at room temperature (RT), forward ET from A_1^- to F_X is characterized by a time constant of ~280 ns (Fig. 2) [18]. As the temperature is lowered ET in PSI becomes heterogeneous, with three distinct processes being observed at 77 K: 1) In ~45% of the PSI particles, $P700^+A_1^-$ recombines with a time constant of ~245 μs at 77 K [18]. This latter time constant was observed for PSI particles from *S. elongatus*. For PSI from *Synechocystis* sp. PCC 6803 (*S6803*) at 77 K, we observe a lifetime of ~300 μs (Fig. 2, and see below). 2) In ~20% of the PSI particles the $P700^+F_x^-$ state forms, and then recombines in the 5–100 ms time range [18]. In ~35% of the PSI particles irreversible charge separation occurs. Spectroscopic signatures associated with this latter fraction are not observable in experiments involving repetitive flash illumination.

The reasons underlying the changes in photochemistry in PSI as the temperature is lowered are not entirely clear. It has been suggested that different conformational substates are frozen below the liquid to glass transition of the medium (~180 K in 65% glycerol) [18]. To further complicate issues, PSI contains two almost identical chains of ET cofactors (Fig. 1), and the degree to which each branch is active in ET is becoming clearer [19,20], with the 280 ns and ~300 μs components at RT and 77 K being associated with ET along the A-branch. It has also been suggested that the ~20% of reaction centers that undergo irreversible ET at 77 K could be associated with ET along the B-branch [21,22].

Often in the literature, the quinone in the A_1 binding site is simply referred to as A_1. Here the quinone in the binding site will be referred to by name, while the term A_1 will be reserved for the actual binding site, thus PhQ occupies the A_1 binding site in regular PSI particles.

It is now well established that the ET cofactors in large photosynthetic protein complexes can be studied in molecular specific detail using light-induced FTIR difference spectroscopy (DS) [23–27]. Much of the work to date utilizes a continuous light-source to photo-accumulate a steady-state population of radical pair states. For example, in PSI the $P700^+F_{A/B}^-$ state recombines in ~80 ms at RT (Fig. 2), and it is straightforward to photo-accumulate a large population of this excited state. For radical pair states with lifetimes in the ~200 ns to ~500 μs range, static excited populations are usually very small, and time resolved (TR) methods are preferred for the collection of FTIR DS associated with the transient species [1]. By far the most widely used approach is time-resolved step-scan (TRSS) FTIR DS [1,28–32].

For PSI photosynthetic protein complexes, bands in the difference spectra have an intensity that is $\sim 1 \times 10^{-3}$ (in absorbance or optical density (OD) units) or less [33,34]. In most cases one is interested in resolving fractional changes in these bands, and for most purposes a sensitivity approaching $1–2 \times 10^{-5}$ is desirable [1]. This is not possible for ns time resolved step-scan (TRSS) FTIR DS, but is possible for microsecond (μs) TRSS FTIR DS. Sensitivity is limited in ns TRSS FTIR DS due mainly to the unavailability of transient digitizers with high dynamic range and bandwidth [1].

Recently, 24-bit transient digitizers with 200 kHz bandwidth have become available, and are standard, or optional, in research grade FTIR instruments. Such digitizers (should) allow very high sensitivity TRSS FTIR measurements with time resolution down to ~5 μs. Some of the work discussed in this review was undertaken using a 24-bit, 200 kHz transient digitizer. In addition, 16 bit, 100 MHz transient digitizers are now available, which may lead to high sensitivity TRSS FTIR measurements with time resolution in the ~10–100 ns range. To date, no ns TRSS FTIR work utilizing such digitizers have been reported.

In a previous review on the use of TRSS FTIR DS for the study of A_1 in PSI [1] information on the instrumentation used for the studies was included, and the reader is referred to that review for further details.

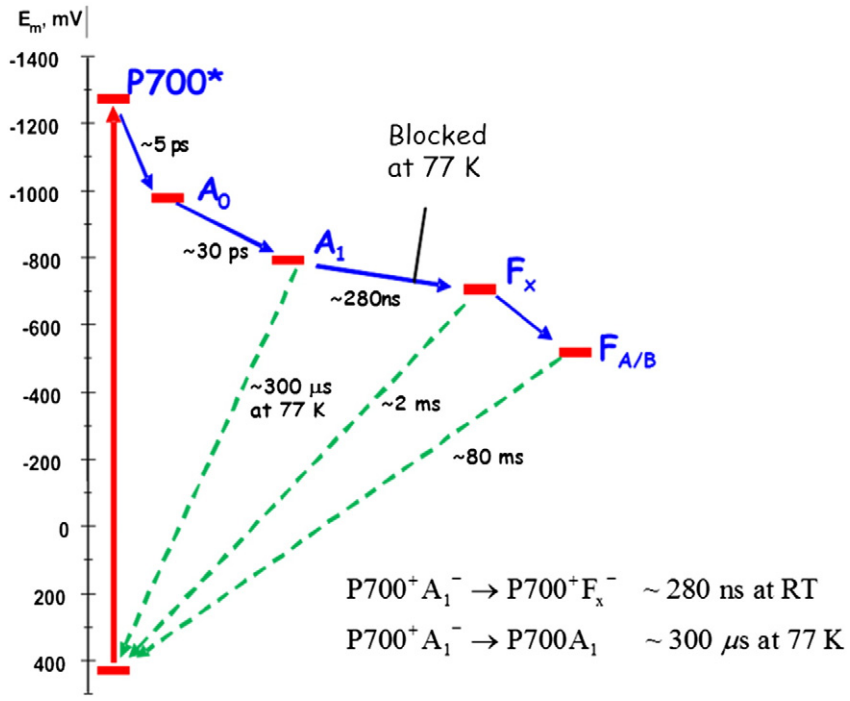

Fig. 2. Energy level scheme showing the kinetics of charge separation in PSI particles at RT and 77 K. Scale indicates approximate reduction midpoint potentials obtained by redox titrations of PSI particles. This figure is a compilation of data, much of which is discussed in previous reviews [9,70].

For PSI, only the ET cofactors P700 and A_1 have been studied using FTIR DS. ($P700^+$–P700) FTIR DS have been produced using (static) photo-accumulation techniques, and several comprehensive reviews of work undertaken to understand the nature of the bands in ($P700^+$–P700) FTIR DS have appeared in the literature, the last being in 2006 [27]. Several works from our group [35–37], and others [38], have appeared since then. Most of this recent work is related to calculation of the normal modes of Chl-*a* molecules in solution, and how the results from these calculations can be used to gain insight into the nature of the bands in ($P700^+$–P700) FTIR DS, and how they are modified upon isotope labeling [35]. In the interests of keeping this review to a manageable size, these most recent works will not be reviewed here.

This review will focus on work undertaken to obtain and interpret TRSS FTIR DS associated with quinones that occupy the A_1 binding site in PSI. In PSI, a PhQ molecule occupies the A_1 binding site. PhQ is a 2-methyl, 3-phytyl, 1, 4 naphthoquinone. The structure and numbering for PhQ is outlined in Fig. 3. As will be discussed further below, other quinones can be incorporated into the A_1 binding site in PSI. So far, TRSS FTIR DS have been obtained for PSI particles with PhQ, plastoquinone 9 (PQ_9), 2-methyl naphthoquinone (2MNQ) and 2-phytyl naphthoquinone (2PhNQ) incorporated into the A_1 binding site. The structure and numbering for these quinones are also outlined in Fig. 3.

The PhQ molecule occupying the A_1 binding site has a midpoint potential close to −800 mV (see [21] for a review). This makes it one of the most reducing quinones in biology. This unprecedented redox potential is in part a result of interactions of PhQ with the surrounding protein environment. The crystal structure of PSI at 2.5 Å resolution [12] provides a detailed view of the amino acids surrounding the PhQ cofactor, and suggests several possible pigment-protein interactions. Fig. 4 shows a view of the PhQ molecule bound to PsaA (denoted A_{1A} in Fig. 1) and several of the surrounding amino acids. The B-side is very similar. The indole ring of TrpA697 (*S. elongatus* numbering) is π-stacked with the PhQ ring plane. The hydroxyl side chain of SerA692 could be hydrogen (H)-bonded to the backbone oxygen of MetA688. MetA688 also ligates the central magnesium atom of the A_0 chlorophyll-a. The indole NH group of TrpA697 may also be H-bonded to the hydroxyl oxygen of SerA692. The crystal structure suggests that the C_1═O group of PhQ is probably not H-bonded whereas the C_4═O is H-bonded to the backbone NH group of LeuA722. Clearly there is an asymmetry in H-bonding to the PhQ C═O groups.

As outlined above, it has not proven possible to study the $P700^+A_1^-$ state using under physiological conditions (at or near RT) using ns TRSS FTIR DS. Femtosecond TR transient absorption spectroscopy (visible pump IR probe) has been used to study PSI particles, and a ($P700^+A_1^-$–$P700A_1$) IR DS was obtained [39]. No further work has been forthcoming in this area, however.

To study the $P700^+A_1^-$ state under non-physiological conditions (at 77 K) only microsecond (µs) TR techniques are required. Sensitivities close to 2×10^{-5} are required, however. This is difficult but achievable using µs-TR FTIR DS. So far, only our research group has produced µs TRSS ($P700^+A_1^-$–$P700A_1$) FTIR DS at 77 K [1].

At the heart of most of the recent FTIR DS work undertaken to study the A_1 binding site is the demonstrated capability of incorporating different quinones into the binding site simply by incubating PSI particles in a molar excess of the quinone of interest. This incubation method for quinone incorporation relies on mutant cells in which genes that code for enzymes involved in PhQ biosynthesis have been disrupted [40,41]. For example, in mutants where the *menB* gene has been deactivated PhQ biosynthesis is inhibited and, perhaps surprisingly, plastoquinone-9 (PQ_9) is recruited into the A_1 site [40–42]. We will refer to PSI particles from these mutant cells as $menB^-$ PSI particles. In $menB^-$ PSI it has been found that foreign quinones can replace PQ_9 in the A_1 binding site, simply by incubating the particles in a large molar excess of the quinone of interest [43–45].

3. ($P700^+A_1^-$–$P700A_1$) and (A_1^-–A_1) FTIR DS at 77 K

Fig. 5A shows TRSS ($P700^+A_1^-$–$P700A_1$) FTIR DS in the 1770–1400 cm^{-1} region obtained using wild type (WT) PSI particles from *S6803*. Also shown are the corresponding spectra obtained using $menB^-$ PSI particles from *S6803* that have been incubated in the presence of PhQ. The spectra for the two samples are very similar, demonstrating that PhQ has been incorporated into the A_1 binding site in $menB^-$ PSI

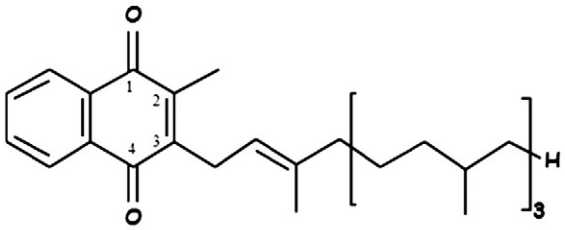

2-methyl, 3-phytyl, 1,4-naphthoquinone
(PhQ)

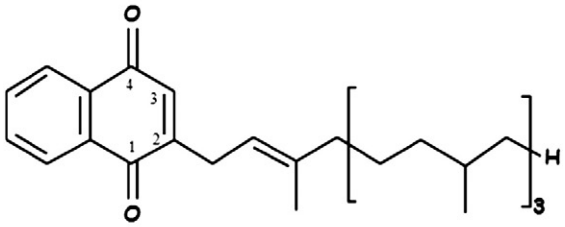

2-phytyl 1,4-naphthooquinone
(2PhNQ)

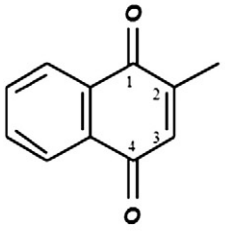

2-methyl 1,4-naphthoquinone
(2MNQ)

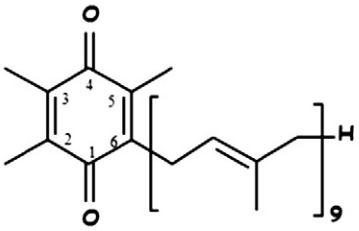

Plastoquinone 9
(PQ_9)

Fig. 3. Structure and numbering scheme for the quinones discussed in this review.

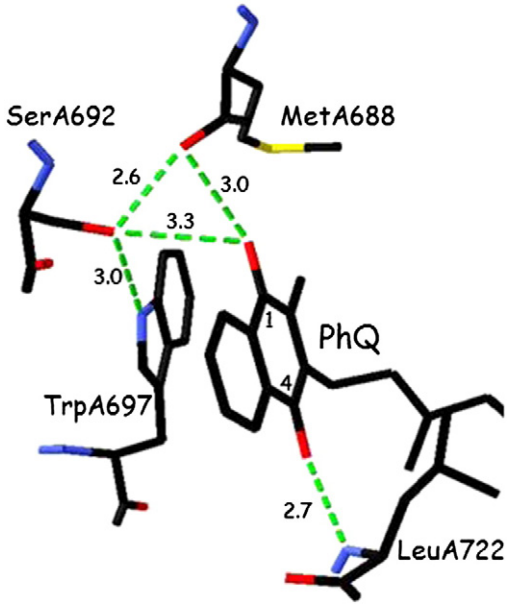

Fig. 4. View of PhQ in the A_{1A} binding site in cyanobacterial PSI. Possible H-bonding interactions of the PhQ carbonyl groups with the protein are shown (*dotted*). Figure was generated from the crystallographic coordinates of PSI at 2.5 Å resolution [PDB file accession number 1JB0] [12]. Nitrogen/oxygen/sulfur/carbon atoms are blue/red/yellow/black, respectively.

particles. The ($P700^+A_1^-$–$P700A_1$) FTIR DS at 77 K shown in Fig. 5A for *menB*$^-$ PSI particles incubated the presence of PhQ is very different to that obtained for straight *menB*$^-$ PSI particles that have not been incubated in the presence of quinones. In this latter case a TR FTIR DS is obtained that is dominated by bands associated with the P700 triplet state (^{3}P700) [43]. The (^{3}P700–P700) FTIR DS displays an intense difference band at 1635(−)/1594(+) cm^{-1}. The lack of such a band in the spectra in Fig. 5A, especially at 1594 cm^{-1}, demonstrates that PhQ added to the buffer is incorporated into the A_1 binding site in nearly all of the reaction centers. Such a high level of incorporation was also indicated from EPR spectroscopic studies [44].

An approach that has been taken in the past is to subtract the static, photo-accumulated ($P700^+$–P700) FTIR DS (also shown in Fig. 5A) from the TR ($P700^+A_1^-$–$P700A_1$) FTIR DS, to produce a so called (A_1^-–A_1) FTIR DS. Such (A_1^-–A_1) FTIR DS obtained using WT and *menB*$^-$ PSI particles are shown in Fig. 5A, and an expanded version is shown in Fig. 5B. Similar spectra have been presented previously for WT PSI particles from *S6803* [1,46], and for *menB*$^-$ PSI particles from *S6803* with PhQ incorporated into the A_1 binding site [43], albeit at a slightly lower signal to noise ratio. When different quinones are incorporated into the A_1 binding site, we have found that in some cases the ($P700^+$–P700) FTIR DS is slightly altered. This observation suggests that in these cases the above describe spectral subtraction is important. However, the applicability of the subtraction depends on the fact that the TR and static ($P700^+$–P700) FTIR DS are identical. By comparing static and TRSS ($P700^+$–P700) FTIR DS at RT we have found that the transient and relaxed spectra are indeed very similar [29], providing some support that this spectral subtraction is appropriate.

To gain an appreciation of the noise level achievable/required for these TRSS FTIR measurements on PSI particles, it is useful to consider the kinetics of the absorption changes at various IR frequencies. Fig. 6 shows the time-course of the absorption changes at 1754, 1748, 1495 and 1415 cm^{-1} for *menB*$^-$ PSI samples with PhQ incorporated. The initial amplitude of the 1754 cm^{-1} time-course is ~2×10^{-4} (in OD units), and the noise level is close to 10^{-5}. No corrections have been applied to the data in Fig. 6. The TRSS data at the four frequencies are fitted simultaneously to a single exponential function (plus a constant), and a lifetime of 304 μs is found, which is similar to that found previously [1,47]. To verify and support the TRSS FTIR data, in our lab we routinely also use ns to ms TR absorption spectroscopy in the visible spectral region, *under identical conditions* to that used in the FTIR measurements (in the FTIR measurements very concentrated protein samples in a very short path-length sample cell are used). The inset in Fig. 6 shows the kinetics of the absorption changes at 703 nm, following 532 nm laser excitation of *menB*$^-$ PSI with PhQ incorporated, at 81 K. Encouragingly, the same time constant (within error) is obtained in both the visible and IR TR measurements.

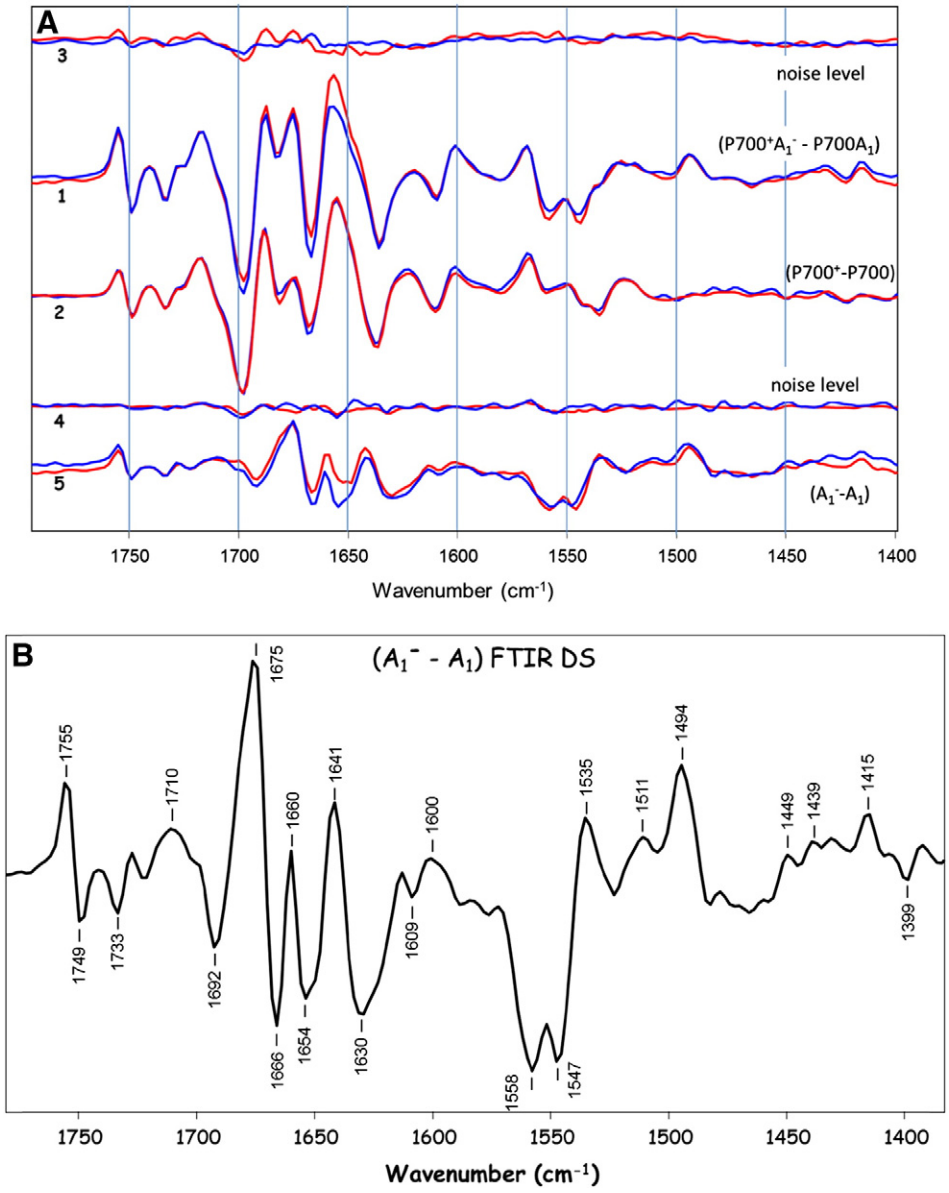

Fig. 5. (A) TRSS ($P700^+A_1^-$–$P700A_1$) (1) and static ($P700^+$–P700) (2) FTIR DS collected at 77 K for WT PSI particles from *S6803* (*red*) and *menB*$^-$ mutant PSI particles from *S6803* that have been incubated in the presence of PhQ (*blue*). Trimeric PSI particles were used in both cases. The spectra shown are the average of up to 9 separate experiments. The standard deviation spectra associated with the time-resolved and static spectra are shown (with same color coding) in (3) and (4), respectively. The TR spectra are the average of 9 spectra collected every 5 μs after the laser flash, and thus are representative of spectra obtained over a 45 μs time period. By subtracting the static ($P700^+$–P700) FTIR DS from the TR ($P700^+A_1^-$–$P700A_1$) FTIR DS, a double difference spectrum (DDS) is constructed, and these spectra are also shown (5) (with same color coding) and are representative of what are called (A_1^-–A_1) TR FTIR DS. The spectra in (5) are similar. (B) Expanded view of the average of the two (A_1^-–A_1) TR FTIR DS shown in (A).

3.1. Origin of the bands in the (A_1^-–A_1) TRSS FTIR DS

3.1.1. Global isotope labeled PSI particles

As a first approach to understanding the nature of the bands in TRSS (A_1^-–A_1) FTIR DS (Fig. 5B) global ^{15}N, ^{13}C and ^2H isotope labeled PSI particles were studied [47]. Based on observed isotope induced band shifts a tentative list of band assignments was suggested. These assignments are outlined in Table 1. Some of these assignments are based on the following criteria:

1) In the simple harmonic oscillator approximation, C═O and C═C modes are expected to downshift ~40 and ~60 cm^{-1}, respectively, upon ^{13}C labeling. For Chl-*a* molecules, 13^3 ester and 13^1 keto C═O modes are expected to downshift ~44 cm^{-1} upon ^{13}C labeling [48].
2) For chlorophyll-*a* molecules, 13^3 ester and 13^1 keto C═O modes are expected to downshift ~6 and ~4 cm^{-1} upon deuteration (^2H labeling) [49].
3) From a consideration of the FTIR absorption spectra for the isotope labeled PSI particles, amide I absorption bands are expected to downshift ~38/0/12 cm^{-1} upon $^{13}C/^{15}N/^2H$ labeling, respectively [47].

Assignments 1 and 2 indicate that the A_0 chlorophyll-*a* pigment is perturbed upon A_1 reduction, presumably via a long range electrostatic interaction. Such electro-chromic effects are entirely reasonable and are expected in PSI, as was discussed previously [1].

Despite the extensive use of global isotope labeling, there is still ambiguity in some of the proposed band assignments, partly because of limited signal to noise ratio in the spectra, and partly because of multiple overlapping spectral features. Upon consideration of FTIR

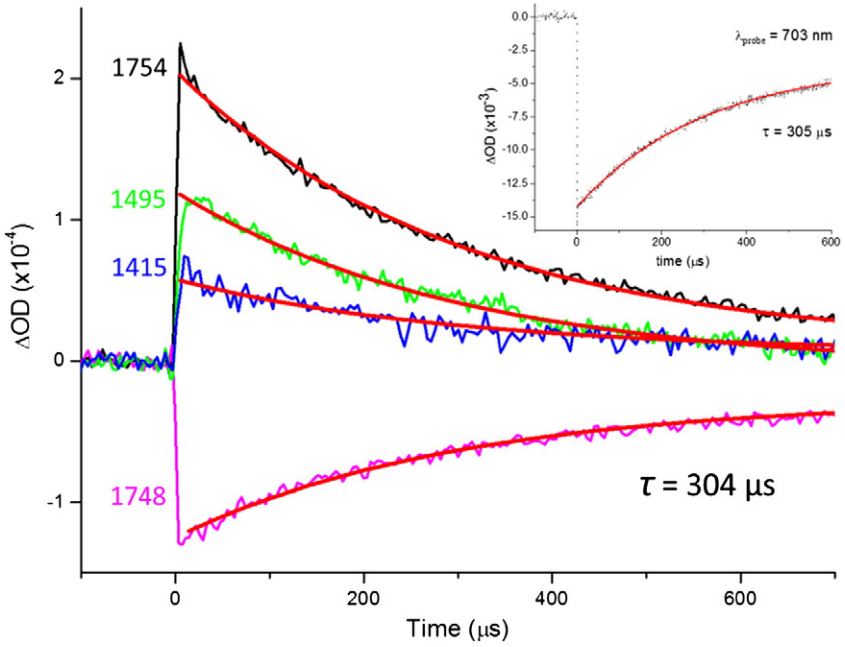

Fig. 6. Kinetics of absorption changes at 1754, 1748, 1495 and 1415 cm^{-1} obtained at 77 K following 532 nm laser flash excitation of *menB*$^-$ PSI particles that have been incubated in the presence of PhQ. Data were collected in 5 μs increments. The four kinetic decays were fitted simultaneously to a single-exponential function plus a constant. The fitted functions are shown (*red*), and are characterized by a time constant of 304 μs. *Inset*: Kinetics of absorption changes at 703 nm obtained at 81 K for the same sample (in the same sample cell) studied using TRSS FTIR DS. The decay was best fitted to a single-exponential function with a time constant of 305 μs.

absorption spectra for PhQ in solution, which show that a PhQ C═O mode is found near 1662 cm^{-1}, and is ~40 cm^{-1} higher than that of bands due to C═C modes [50], it is unlikely that assignment 5 in Table 1 is correct. In addition, the 1415 cm^{-1} band was suggested to downshift 58 cm^{-1} upon ^{13}C labeling. Given this hypothesis the 1415 cm^{-1} band was suggested to be due to a $C\!=\!C$ mode of PhQ^-. Later work (discussed below) indicates that the 1415 cm^{-1} mode may contain a small contribution from $C\!=\!C$ groups, but the mode is considerably more complicated, and a 58 cm^{-1} ^{13}C induced band shift is unlikely.

3.1.2. Vibrational frequency calculations

Up until ~2005, computational studies (vibrational frequency calculations) were rarely undertaken in parallel with experiment, to assess whether proposed assignment of bands in FTIR DS were reasonable. To address this issue, Bandaranayke et al. [50] undertook density functional theory (DFT) based vibrational frequency calculations (at the B3LYP 6–31G+(d) level) for neutral and reduced, unlabeled, ^{13}C, ^{2}H and ^{18}O isotope labeled PhQ in the gas phase. Calculations for PhQ in solvent (using the integral equation formalism of the polarized continuum model IEF PCM) (G. Hastings, unpublished data), and using higher levels of theory [50], leads to the same conclusions as that presented in reference [50].

Although calculations were undertaken only for gas phase PhQ, some trends were noted and could be usefully applied to a consideration of experimental (A_1^-–A_1) FTIR DS (Fig. 5B):

1. C═O modes of PhQ absorb ~40 cm^{-1} higher in frequency than quinonic C═C modes of PhQ. However, $C\!=\!O$ modes of PhQ^- absorb ~23 cm^{-1} *lower* in frequency than $C\!=\!C$ modes. If the 1494(+) cm^{-1} band in Fig. 5B is due to a $C\!=\!C$ mode of PhQ^-, then this calculated prediction could indicate that at least part of the 1511(+) cm^{-1} band (or the poorly resolved shoulder near 1516 cm^{-1}) could be due to a $C\!=\!C$ mode of PhQ^-.
2. Deuteration (^2H) induced shifts of C═O and C═C modes are very different for neutral and reduced PhQ [50]. It is calculated that the C═O/C═C modes of neutral PhQ will downshift 2/11 cm^{-1}, while $C\!=\!O$/$C\!=\!C$ modes of PhQ^- will downshift 18/26 cm^{-1}, upon deuteration. This is a clear indication that $C\!=\!O$/$C\!=\!C$ modes of PhQ^- are considerably mixed with C–H bending vibrations, unlike the corresponding modes of neutral PhQ. Although these calculated results seem useful, utilizing this information to identify bands in the experimental spectra is still fraught with difficulty and, of course, if the C═O modes are also hydrogen (H) bonded this will further complicate analysis of any ^2H induced frequency shifts.

Following on from these calculations for PhQ and PhQ^- in the gas phase, later calculations included molecular groups that were H-bonded to the C_4═O group of PhQ [46,51]. This was done specifically in an attempt to better simulate the vibrational properties of the quinone occupying the A_1 binding site in PSI (Fig. 4).

4. PSI with different quinones incorporated into the A_1 binding site

One way to test the validity of the band assignments listed in Table 1 is to study PSI particles in which the PhQ in the A_1 binding site has been replaced with a closely related analogue, or by a completely different quinone, or by an isotope labeled version of PhQ. By monitoring how

Table 1
Assignments proposed for bands in unlabeled (A_1^-–A_1) FTIR DS. Assignments were proposed upon consideration of spectra obtained using unlabeled, ^{13}C, ^{2}H and ^{15}N labeled PSI particles [47], as well as studies of site directed mutants [69]. Table entries in italics are questionable, as discussed in the text. Hypothesis for alternative assignments are also discussed in the text.

1	1754(+)/1749(−)	13^3 ester C═O of A_0
2	1692(−)/1675(+)	13^1 keto C═O of A_0
3	1666(−)1675(+)	amide I mode
4	1654(−)	C_1═O mode of neutral PhQ
5	*1650(−)*	*C═C mode of neutral PhQ*
6	1630(−)[a]	C═C mode of neutral PhQ[a]
7	*1607(−)*	*C_4═O mode of neutral PhQ*[b]
8	1558(−)/1547(−)	amide II
9	1494(+)	$C\!=\!O$ mode of PhQ^-
10	*1415(−)*	*$C\!=\!C$ mode of PhQ^-*

[a] Only part of the band. Amide I modes may also contribute to this band.
[b] Very weak feature that is close to the noise level.

bands shift in (A_1^-–A_1) FTIR DS obtained with these altered PSI particles one can assess the appropriateness of the above listed assignments. Such experiments could also provide information on new possible band assignments.

As mentioned above, this approach for studying PSI particles with modified or different quinones incorporated into the A_1 binding site became an attractive possibility with the creation of mutant cyanobacterial cells in which the genes that code for enzymes involved in PhQ biosynthesis were disrupted/inactivated. Various mutant cell lines have been produced when various genes were disrupted, giving rise to the so-called *men* (men is an abbreviation for menaquinone) mutants [40,41,52–55].

In *menB*, *D* and *E* mutant cells, PhQ biosynthesis is inhibited and a PQ_9 molecule is recruited into the A_1 binding site [40,41]. The structure and numbering for PQ_9 is outlined in Fig. 3.

The *menG* gene codes for a methyl-transferase. Inactivation of the *menG* gene leads to the synthesis of a PhQ analogue that lacks a 2-methyl group. This PhQ analogue is incorporated into the A_1 site in PSI, and it functions nearly as effectively as PhQ in WT cells [54]. Cells in which the *menG* gene is inactivated will be called *menG*$^-$ cells below. In *menG*$^-$ cells, a PhQ analogue in which the methyl group (of PhQ) is replaced with a hydrogen atom occupies the A_1 binding site [54]. Here this methyl-less PhQ analogue is referred to as 2PhNQ (as an abbreviation for 2-phytyl naphthoquinone) (Fig. 3). The loss of the methyl group will alter the electronic structure of the naphthoquinone (NQ) headgroup, which is expected to lead to altered frequencies of some of the bands in the (A_1^-–A_1) FTIR DS.

4.1. Incorporation of 2PhNQ into the A_1 binding site in PSI

TRSS (A_1^-–A_1) FTIR DS have been obtained using *menG*$^-$ PSI particles at 77 K. In addition, vibrational frequency calculations comparing 2PhNQ and PhQ (in the gas phase) have been undertaken [46]. In an attempt to more accurately simulate the vibrational properties of quinones in the A_1 binding site (Fig. 4), sets of calculations were also undertaken for PhQ and 2PhNQ in the presence of an H-bond to the C_4═O group provided by either a water molecule or the backbone NH group of a truncated leucine residue. Note that in these and previous vibrational frequency calculations the phytyl chain is truncated to only a single phytyl unit, with the rest of the chain being replaced by a hydrogen atom. We have found that inclusion of more than one phytyl unit does not lead to significant modification of the vibrational mode frequencies or intensities associated with groups of the NQ ring (not shown).

Experimentally it is found that the PhQ^- band at 1494 cm^{-1} in Fig. 5B up-shifts to ~1498 cm^{-1} when 2PhNQ is incorporated into the A_1 binding site. Interestingly, the band at 1415 cm^{-1} is unaltered. Comparison of the experimental results with vibrational frequency calculations indicated that the shift of 1494 cm^{-1} band was compatible with it being due to a $C\!=\!O$ mode of PhQ^- in the A_1 binding site. The lack of any shift of the 1415 cm^{-1} band (found experimentally), is also compatible with vibrational frequency calculations. The calculations show that the 1415 cm^{-1} band (calculated at an unscaled frequency of 1471 cm^{-1} for PhQ in the gas phase [46]) is due to C – H bending vibrations that are weakly coupled to aromatic $C\!=\!C$ stretching and antisymmetric $C\!=\!O$ stretching vibrations. Such a complex mode description is also appropriate when the C_4═O group is H-bonded [46]. Thus assignment 10 in Table 1 gives an incomplete description of the nature of the vibrational mode responsible for the 1415 cm^{-1} band. Assignment 10 in Table 1 was based on a hypothesized ^{13}C induced downshift of 58 cm^{-1} for the 1415 cm^{-1} band. If the calculated mode description for the 1415 cm^{-1} band is appropriate, then there is no possibility that it will downshift 58 cm^{-1} upon ^{13}C labeling, and hence the hypothesized/suggested ^{13}C induced downshift of the 1415 cm^{-1} band [47] is incorrect.

The (A_1^-–A_1) FTIR DS for *menG*$^-$ mutant PSI displays some quite considerable alterations compared to WT PSI. These alterations appear to emanate from altered amide I and II vibrational modes. This might suggest some change in the orientation of 2PhNQ in the A_1 binding site relative to PhQ. However, magnetic resonance studies argue against this hypothesis as they showed that 2PhNQ is oriented in the A_1 binding site in a similar manner to PhQ [54].

Although it was suggested to be the case, the data in Ref. [46] are *not* consistent with the idea that a band at 1654 cm^{-1} is due to a C═O mode of neutral PhQ. For PhQ in THF, the antisymmetric C═O mode (antisymmetric vibration of both C═O groups) occurs at ~1662 cm^{-1} [51]. So for PhQ in the A_1 binding site in PSI, C═O modes are likely to be found at frequencies below 1662 cm^{-1}. Since 2PhNQ C═O modes are calculated to be ~7 cm^{-1} higher in frequency than for PhQ, one expects C═O modes of 2PhNQ in the A_1 binding site to be found at frequencies below ~1669 cm^{-1}. From (*menG*$^-$–WT) FTIR double difference spectra (DDS) [46], there are no obvious bands that point to the vibrational frequencies of the C═O groups of either PhQ or 2PhNQ.

4.2. Incorporation of ^{18}O isotope labeled PhQ into the A_1 binding site in PSI

^{18}O labeled PhQ has been incorporated into *menB*$^-$ PSI, and by comparing (A_1^-–A_1) FTIR DS for PSI with unlabeled and ^{18}O labeled PhQ incorporated an (^{18}O–^{16}O) FTIR DDS has been produced [51]. In these measurements, in most of the RC's, both oxygen atoms of the quinone are ^{18}O labeled, and the extent of incorporation of the ^{18}O label into PhQ is ~70% [51]. Since P700 (and/or nearby amide modes) will not be impacted by ^{18}O labeling of PhQ, there is no need to subtract ($P700^+$–P700) FTIR DS from ($P700^+A_1^-$–$P700A_1$) FTIR DS to produce (A_1^-–A_1) FTIR DS. With this in mind, Fig. 7A shows TRSS ($P700^+A_1^-$–$P700A_1$) FTIR DS obtained using PSI particles with unlabeled (^{16}O) and ^{18}O labeled PhQ incorporated into the A_1 binding site. The (^{18}O–^{16}O) FTIR DDS is also shown. The DDS shown in Fig. 7A is similar to that presented previously [51].

For (^{18}O–^{16}O) FTIR DDS, in the neutral quinone spectral region (1770–1550 cm^{-1}), bands of unlabeled PhQ are positive while bands of ^{18}O PhQ are negative. In the anion spectral region (1550–1350 cm^{-1}), bands of unlabeled PhQ^- are negative while bands of ^{18}O PhQ^- are positive.

As indicated previously, and as is also clear in the DDS in Fig. 7B, a band at 1495 cm^{-1} in the ^{16}O spectrum downshifts 14 cm^{-1} to 1481 cm^{-1} in the ^{18}O spectrum. If the 1495 cm^{-1} band is due to a $C\!=\!O$ mode of PhQ^- then the next question is: Should such a mode downshift only 14 cm^{-1} upon ^{18}O labeling?

In the simple harmonic oscillator approximation, a C═O mode at 1650–1495 cm^{-1} is expected to downshift 36–40 cm^{-1}. From DFT based vibrational frequency calculations, however, C═O modes of neutral PhQ are found to downshift ~29 cm^{-1}. A 29 cm^{-1} ^{18}O induced downshift is in good agreement with experimental FTIR absorption spectra for ^{16}O and ^{18}O labeled neutral PhQ in solution (THF) [51].

For PhQ^-, however, $C\!=\!O$ modes are calculated to downshift ~14 cm^{-1} upon ^{18}O labeling. Thus the ^{18}O induced downshift of a $C\!=\!O$ mode of PhQ^- is half that of a C═O mode of neutral PhQ. Part of the reason for a smaller ^{18}O induced downshift for $C\!=\!O$ modes of PhQ^- is that these modes are more strongly coupled to C – H bending vibrations than are the corresponding modes in the neutral state.

From DFT based vibrational frequency calculations for PhQ^- with the C_4═O group H-bonded to the backbone NH of a leucine residue, it was predicted that there would be only one intense antisymmetric coupled $C\!=\!O$ stretching vibration, unlike the case for the neutral state of PhQ, where it is calculated that the C═O modes uncouple upon asymmetric H-bonding [51]. Fig. 7B shows a calculated DDS obtained from an ONIOM type, QM/MM calculation for PhQ in the A_1 binding site. The calculated spectrum is very similar to that found previously [51], and the modes giving rise to the features in the spectrum are also similar to that derived previously.

What could not be ascertained with confidence previously was what happened to the 1415 cm^{-1} band upon ^{18}O labeling of PhQ. This is clear in Fig. 7B, however, where it is shown that the band at 1415 cm^{-1} downshifts 6 cm^{-1} upon ^{18}O labeling. This downshift is about half that

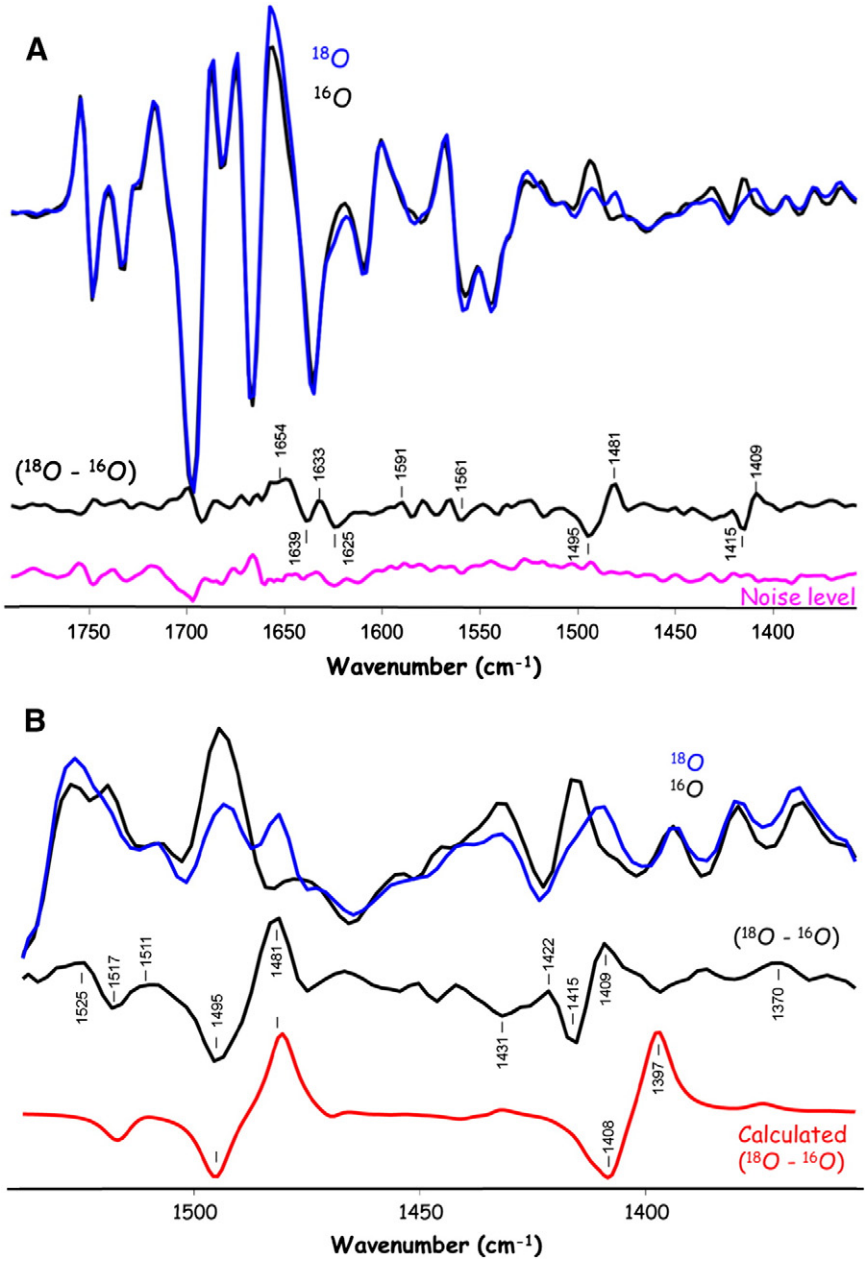

Fig. 7. (A) TRSS ($P700^+A_1^-$–$P700A_1$) FTIR DS collected at 77 K for *menB*$^-$ PSI particles with unlabeled (^{16}O) (*black*) and ^{18}O labeled (*blue*) PhQ incorporated into the A_1 binding site. The spectra shown are the average of 9 and 4 separate experiments, respectively. A spectrum that shows the standard deviation associated with the 4 "^{18}O labeled" spectra that are averaged is also shown. These standard deviation spectra give one measure of the experimental variability (noise level) inherent in these measurements. The TR spectra shown are the average of 9 spectra collected in 5 μs increments following a ~5 ns, 532 nm laser flash. By subtracting the ^{16}O spectrum from the ^{18}O spectrum a (^{18}O–^{16}O) FTIR DDS is constructed, and this spectrum is also shown. (B) Expanded view of the spectra in (A) in the PhQ anion spectral region (1550–1350 cm^{-1}). Also shown is a calculated (^{18}O–^{16}O) DDS (*red*, *bottom*).

expected for a PhQ^- C⩵O mode. This observed downshift indicates that the 1415 cm^{-1} band is due to a mixed mode with some C⩵O character. In the above discussion it was concluded (from computational work) that the 1415 cm^{-1} band is due to a mode consisting of C – H bending vibrations that are weakly coupled to C⩵C stretching and antisymmetric C⩵O stretching vibrations. The observed 6 cm^{-1} ^{18}O induced downshift of the 1415 cm^{-1} band seems to support this calculated mode composition. The similarity in the calculated and experimental DDS (Fig. 7B) suggests that the computational approach employed is appropriate.

The DDS in Fig. 7B suggest the presence of a negative band at ~1517 cm^{-1}, that may downshift ~6 cm^{-1} upon ^{18}O labeling. Above it was suggested that a band at 1511 cm^{-1} (or shoulder at 1516 cm^{-1}) in Fig. 5B might be due to a PhQ^- C—C mode. Thus the negative band at 1517 cm^{-1} (Fig. 7B) may be due to a PhQ^- C—C mode with some C⩵O character.

Of the TRSS FTIR DS that have been produced so far, one major difficulty has been the unambiguous identification of bands associated with neutral PhQ. Part of the difficulty is that the C═O bands of PhQ overlap amide I absorption bands, making an unambiguous identification difficult. It is becoming clear, however (see above), that a C═O mode of neutral PhQ gives rise to a feature near ~1654 cm^{-1}. The positive feature near 1654 cm^{-1} in the DDS in Fig. 7A is therefore associated with a C═O mode of neutral PhQ. What happens to this 1654 cm^{-1} feature upon ^{18}O labeling, is not entirely clear. The most likely possibility is that the 1654 cm^{-1} feature downshifts 29 cm^{-1} to 1625 cm^{-1} upon

^{18}O labeling. This hypothesis was suggested previously from the DDS [51], and in part because it is the predicted ^{18}O induced downshift for a non-H-bonded C═O mode of neutral PhQ [51].

One complication in the DDS in Fig. 7A is the origin of the positive 1633 cm^{-1} feature. This feature was not discussed previously, as there was only a suggestion of a positive shoulder near 1633 cm^{-1} in the DDS [51]. The 1633 cm^{-1} feature could be due to a (H-bonded) C═O mode of neutral PhQ. Of course, if this is true then the question of where this band shifts to upon ^{18}O labeling arises. One would expect a C═O band at 1633 cm^{-1} to downshift ~29 cm^{-1} to ~1604 cm^{-1} upon ^{18}O labeling. Unfortunately, there is no clear indication in the DDS in Fig. 7A for a negative band near 1604 cm^{-1}.

On the basis of isotope induced frequency shifts, a band at ~1607 cm^{-1} in (A_1^-–A_1) FTIR DS for WT PSI was tentatively assigned to the C═O group of PhQ that is H bonded to the backbone NH of a leucine residue (Table 1) [47]. TRSS FTIR studies of the *menG*$^-$ PSI samples found no strong evidence for a band at ~1607 cm^{-1} that could be associated with an H-bonded C═O group, however. The specific ^{18}O isotope labeled PhQ data also provides no support for this hypothesis, so assignment 7 in Table 1 appears questionable.

Based on the data that has been presented in the literature so far, and which has been discussed above, it is fair to say that there has been no unambiguous identification of a band that could be associated with an H-bonded C═O group of neutral PhQ in the A_1 binding site (although see below).

4.3. Incorporation of 2MNQ into the A_1 binding site in PSI

To gain more information on the nature of bands in TRSS ($P700^+A_1^-$–$P700A_1$) FTIR DS, one approach is to compare spectra for PSI with different PhQ analogues incorporated into the A_1 binding site. For example, to investigate how the phytyl tail of PhQ influences the spectra one could try to substitute in 2MNQ, a PhQ analogue that lacks the phytyl tail (Fig. 3).

TRSS (A_1^-–A_1) FTIR DS at 77 K for *menB*$^-$ PSI particles with 2MNQ incorporated into the A_1 binding have been presented previously, but only in the anion spectral region (1545–1400 cm^{-1}) [56]. In this preliminary study TRSS (A_1^-–A_1) FTIR DS at 77 K for *menB*$^-$ PSI particles with specifically $^{13}C_1$ and $^{13}C_4$ labeled 2MNQ were also presented [56]. No followup work has been reported, however.

Recently work in our lab has begun to focus on the incorporation of 2MNQ into the A_1 binding site in PSI, and Fig. 8A shows TRSS ($P700^+A_1^-$–$P700A_1$) FTIR DS collected at 77 K for PSI particles with PhQ or 2MNQ incorporated into the A_1 binding site. The (2MNQ–PhQ) DDS is also shown in Fig. 8A, along with an estimate of the experimental variability. Fig. 8B shows and expanded view of the DDS in the anion spectral region, along with the calculated DDS obtained from DFT based vibrational frequency calculations of PhQ^- or $2MNQ^-$ with the C_4═O H-bonded to the NH group of the peptide backbone of a truncated leucine residue.

4.3.1. Forward ET and recombination reactions in PSI with 2MNQ incorporated

Before discussing the spectra in Fig. 8 it is important to asses to what extent 2MNQ is incorporated into the A_1 binding site in *menB*$^-$ PSI. Usually, *menB*$^-$ PSI samples are incubated in the presence of a ~100 fold molar excess of the quinone of interest, and previous EPR studies have suggested a very high degree of incorporation of 2MNQ into *menB*$^-$ PSI [57]. In our lab we use ns to ms-TR absorption spectroscopy (in the visible spectral region, probing at 487, 703 or 800 nm) to assess quinone incorporation levels. For PSI with PhQ in the A_1 binding site, radical pair recombination at RT is characterized by a time constant greater than 80 ms (Fig. 2). For *menB*$^-$ PSI, with PQ_9 in the A_1 binding site, the time constant is found to be ~3 ms [42,58,59]. How these time constants relate to the redox potential of the quinone in the binding site has been discussed [21,59].

The RT flash-induced absorption changes at 703 nm for PSI with 2MNQ incorporated is shown in Fig. 9B, and indicates that the $P700^+A_1^-$ state recombines in 14.4 ms. This result has never been reported in the literature, although it has been mentioned in a thesis dissertation [44]. The observation that $P700^+A_1^-$ recombines in 14.4 ms, and not ~3 or 80 ms, is a clear indication that 2MNQ is incorporated into the A_1 binding site. Given that nearly all of the bleaching at 703 nm recovers with a 14.4 ms lifetime (Fig. 9B), it is reasonable to conclude that 2MNQ is incorporated into nearly all of the *menB*$^-$ PSI particles.

Fig. 9A shows the RT flash-induced absorption changes at 487 nm. Flash induced, RT absorption changes at 487 nm is used to probe forward ET from A_1^- to F_x [60,61]. For PSI with PhQ/PQ_9 in the A_1 binding site forward ET (at RT) is characterized by time constants of ~280 ns [18,60]/~15 μs [42], respectively. That is, forward ET is ~50 times slower for PSI with PQ_9 in the A_1 binding site compared to WT PSI with PhQ in the A_1 binding site.

Forward ET rates for *menB*$^-$ PSI with 2MNQ incorporated into the A_1 binding site have not been reported, but the data in Fig. 9A indicate the lifetime is ~3.4 μs. This measured lifetime can be used to estimate the redox potential of 2MNQ in the A_1 binding site, but such a discussion will considerably digress from the subject matter at hand.

Fig. 9 also shows 77 K flash-induced absorption changes at 703 nm (D) and at several frequencies in the IR (C) for *menB*$^-$ PSI with 2MNQ incorporated into the A_1 binding site. Time constants of 221 μs (C) or 206 μs are calculated, which are essentially the same within the noise level of the experiment. This 206–221 μs time constant is indicative of recombination of the $P700^+A_1^-$ state, and is roughly 100 μs faster than that found for PSI with PhQ in the A_1 binding site (Fig. 6). The fact that the two TR approaches (Fig. 9C and D) give similar results is encouraging. The fact that the different recombination lifetimes for PSI with 2MNQ or PhQ in the A_1 binding site are well resolved using TRSS FTIR DS is also encouraging.

4.3.2. TRSS FTIR DS for PSI with 2MNQ in the A_1 binding site

For the (2MNQ–PhQ) DDS in Fig. 8A, in the neutral quinone spectral region (1770–1550 cm^{-1}), 2MNQ bands are negative while bands of PhQ are positive. In the anion spectral region (1550–1400 cm^{-1}), bands of $2MNQ^-$ are positive while bands of PhQ^- are negative.

One striking feature in the DDS in Fig. 8A is that there are many bands, particularly in the 1770–1600 cm^{-1} region, where amide I protein bands, and bands associated with neutral quinones, predominate. This suggests that the phytyl chain leads to some modification of the protein environment surrounding the quinone, but possibly also in the protein environment surrounding P700 (by subtracting ($P700^+A_1^-$–$P700A_1$) FTIR DS to produce DDS, contributions from alterations in P700 due to quinone exchange will also contribute to the DDS). Analysis of the features in the DDS in the neutral region (~1770–1600 cm^{-1}) is therefore complex and poorly understood at present. On the other hand, one very interesting feature in the DDS in Fig. 8A is the difference band at 1633(+)/1640(−) cm^{-1}. This could suggest an H-bonded C═O mode of neutral PhQ at 1633 cm^{-1}, with the corresponding mode of 2MNQ at 1640 cm^{-1}. It was suggested above that a 1633(+) cm^{-1} feature in the DDS in Fig. 7A could be due to H-bonded C═O mode of neutral PhQ. This latter suggestion was not without problems, however, so it is still fair to say that the vibrational frequency of the H-bonded C═O group of neutral PhQ in the A_1 binding site has not been established unambiguously.

Analysis of the absorption changes in the anion spectral region (1550–1400 cm^{-1}) of the DDS in Fig. 8B appear less convoluted. One prominent observation in the DDS is the 1494(−)/1504(+) cm^{-1} derivative feature. As discussed above, the 1494 cm^{-1} band is due to a PhQ^- $C{=}O$ mode, which appears to upshift to 1504 cm^{-1} upon removal of the phytyl tail of PhQ. Thus, with 2MNQ in the A_1 binding site, a $C{=}O$ mode of $2MNQ^-$ appears at 1504 cm^{-1}, 10 cm^{-1} higher than the corresponding mode of PhQ^-. This result is in good agreement with

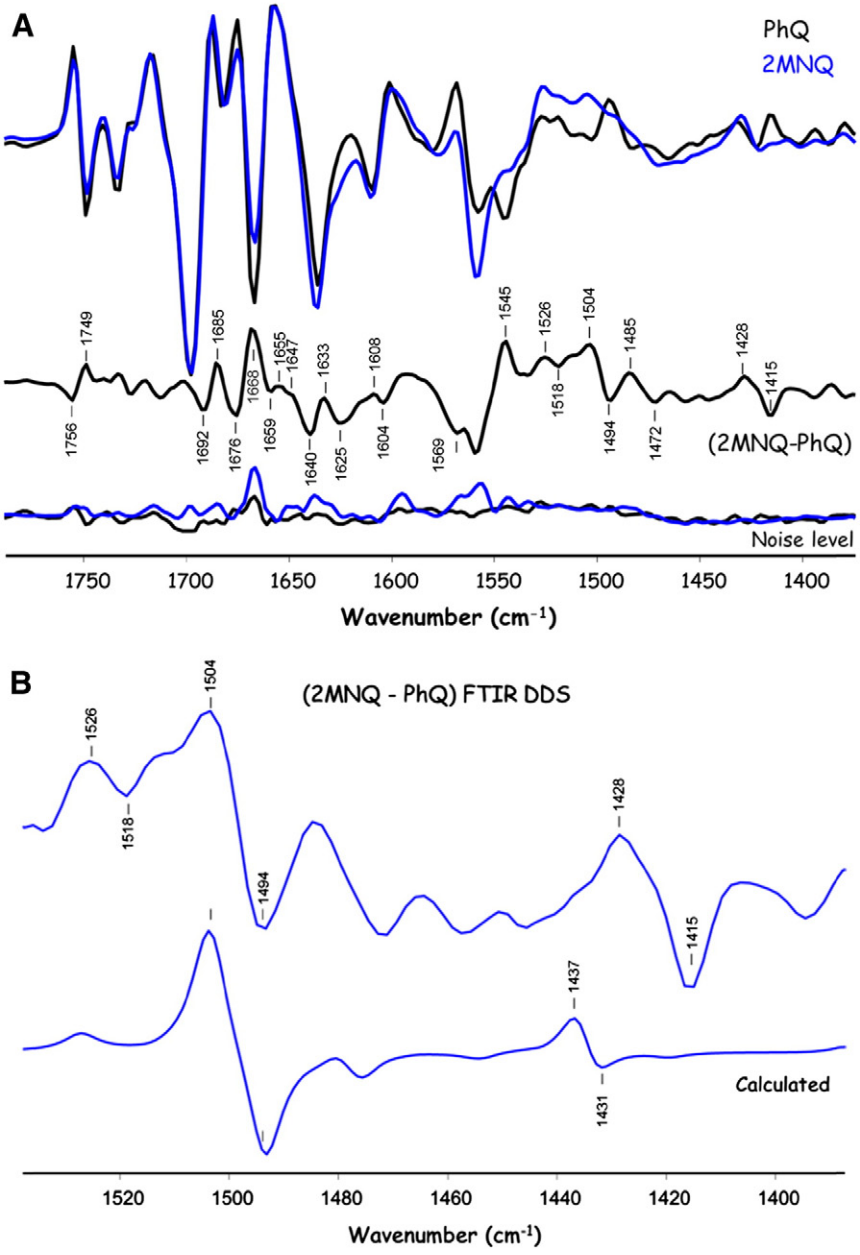

Fig. 8. (A) TRSS ($P700^+A_1^-$–$P700A_1$) FTIR DS collected at 77 K for *menB*$^-$ PSI particles with PhQ (*black*) or 2MNQ (*blue*) incorporated into the A_1 binding site. The spectra shown are the average of 9 and 10 separate experiments, respectively. Spectra that show the standard deviation associated with the (9 or 10) averaged spectra are also shown (with same color coding). These standard deviation spectra give a true measure of the experimental variability (noise level) in these measurements. Such spectra are rarely reported, simply because these types of experiments are rarely repeated a large number of times. Each of the TRSS FTIR DS that were initially averaged are the average of 9 spectra collected in 5 μs increments following a 532 nm laser flash, as described above. By subtracting the "PhQ spectrum" from the 2MNQ spectrum a (2MNQ–PhQ) FTIR DDS is constructed. (B) Expanded view of the DDS shown in (A). A calculated DDS is also shown. The molecular model used for this calculation is similar to that shown in Fig. 3 of reference [51], and consists of a PhQ molecule with the C_4═O group H-bonded to the backbone NH of a truncated leucine residue.

DFT based vibrational frequency calculations for PhQ^- and $2MNQ^-$ in the gas phase [56].

Another clear feature in the DDS in Fig. 8B is the derivative feature at 1415(−)/1428(+) cm^{-1}. As discussed above, for PhQ in the A_1 binding site, the feature at 1415 cm^{-1} has been assigned to a mode in which C⋍O and C=C stretching vibrations are coupled to C–H bending vibrations. The DDS indicates that this mode is at 1428 cm^{-1} for $2MNQ^-$. That is, replacement of the phytyl tail of PhQ with an H atom results in a 13 cm^{-1} upshift of this mode. DFT based vibrational frequency calculations for non-H-bonded PhQ^- and $2MNQ^-$ in the gas phase appear to indicate that a band of PhQ^- *downshifts* 7 cm^{-1} upon replacement of the phytyl chain of PhQ^- with an H atom, however [56]. Clearly, these gas phase calculations inadequately model this aspect of the experimental spectra.

The calculated spectrum outlined in Fig. 8B, which considers H-bonded quinones, indicates a band of $2MNQ^-$ at 1437 cm^{-1}, with the corresponding band for PhQ^- being 6 cm^{-1} lower. This latter calculation agrees with the experimental spectra. So calculations that include an H-bond to the C_4═O group are required to adequately model this aspect of the experimental spectra. The calculated band frequencies, their relative intensities, as well as the shift expected when 2MNQ is incorporated, do not match the experiment particularly well, however. Clearly, even more sophisticated vibrational frequency calculations are required, and such QM/MM type ONIOM calculations are beginning in our lab.

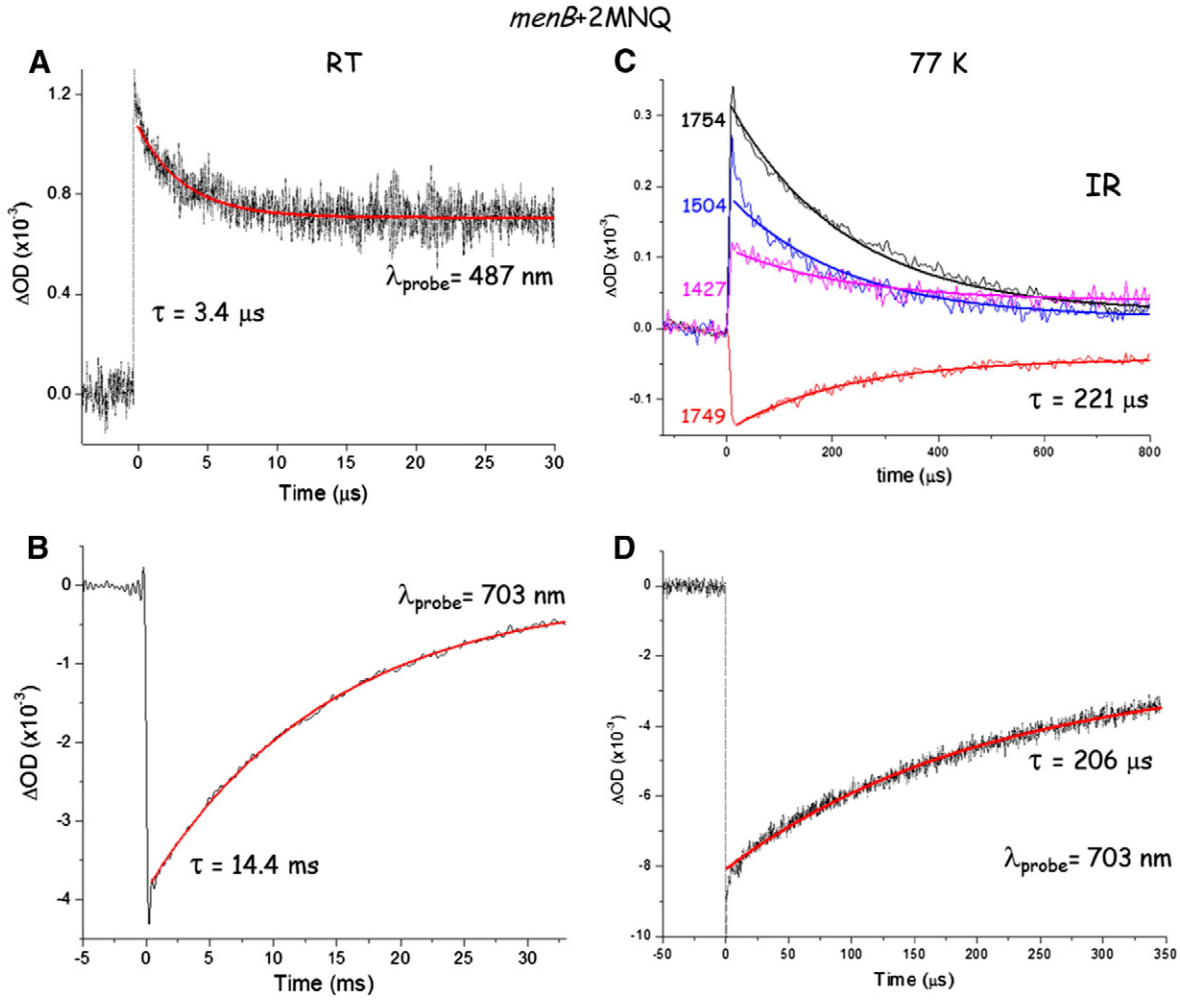

Fig. 9. Flash induced absorption changes for *menB*$^{-}$ PSI with 2MNQ incorporated, at RT (*left*) and 77 K (*right*). (A) Probing forward ET at 487 nm. (B) Probing radical pair ($P700^{+}F_{A/B}^{-}$) recombination at 703 nm. (D) Probing radical pair ($P700^{+}A_{1}^{-}$) recombination at 703 nm. (C) IR absorption changes at 1754, 1749, 1504 and 1427 cm^{-1}. In each of the four captions, the absorption changes were fitted to a single-exponential function plus a constant. The fitted functions are shown (*red*). Time constant obtained are 3.4 μs/14.4 ms/221 μs/206 μs in A/B/C/D, respectively. The four IR decays in C were fitted simultaneously assuming the same time constant at each frequency.

The DDS in Fig. 8B display a derivative feature at 1472(−)/1485(+) cm^{-1}. This feature may indicate a band of PhQ^{-} at 1472 cm^{-1} with a corresponding band in $2MNQ^{-}$ at 1485 cm^{-1}. It is difficult to infer the presence of a PhQ^{-} band at 1472 cm^{-1} from the DDS in Fig. 7, however.

Another feature in the DDS in Fig. 8B is the negative/positive band at 1518/1526 cm^{-1}, possibly indicating a band of PhQ^{-} at 1518 cm^{-1} with a corresponding band in $2MNQ^{-}$ at 1526 cm^{-1}. This proposal is in line with the DDS in Fig. 7, where a negative feature appears at 1517 cm^{-1}, downshifting to 1511 cm^{-1} upon ^{18}O labeling. A band of PhQ^{-} at ~1517 cm^{-1} may also be compatible with the (A_1^{-}–A_1) FTIR DS in Fig. 5B, which displays a positive shoulder at ~1517 cm^{-1}. As suggested above, the feature near 1517 cm^{-1} may be due to a PhQ^{-} $C{=}C$ mode with some $C{=}O$ character. This proposal is consistent with DFT based vibrational frequency calculations, where it is known that $C{=}C$ modes (of PhQ^{-} and $2MNQ^{-}$) are higher in frequency than $C{=}O$ modes.

5. Vibrational spectroscopic properties of quinones occupying other protein binding sites

To gain a more detailed understanding of the vibrational spectroscopic properties of quinones in the A_1 binding site in PSI, it is useful to also consider work undertaken to study quinones in other protein binding sites. In particular, much work (both computational and experimental) has been undertaken to investigate the vibrational spectroscopic properties of quinones occupying the Q_A binding site in purple bacterial reaction centers (PBRCs) from *Rhodobacter* (*Rb.*) *sphaeroides*. In WT PBRCs from *Rb. sphaeroides* ubiquinone-10 (UQ) occupies the Q_A binding site. Fig. 10 shows a structural model of UQ in the Q_A binding site. UQ is a 2,3-dimethoxy, 5-methyl, 6-isoprenoid, 1,4-benzoquinone. For UQ in the Q_A binding site the $C_1{=}O$ is H-bonded to the backbone NH group of AlaM260. The $C_4{=}O$ is H-bonded to the imidazole NH group of HisM219. This imidazole also ligates the non-heme iron atom.

Comparing Figs. 10 and 4 it seems there are similarities in quinone binding in the Q_A and A_1 sites. From simply comparing the structures, however, it is difficult to assess if UQ in the Q_A binding site is more or less symmetrically H-bonded than PhQ in the A_1 binding site. This question has been addressed from the vantage point of EPR spectroscopic studies [57], which suggests that PhQ^{-} in PSI is very asymmetrically H-bonded (perhaps even only the $C_4{-}O$ group of PhQ^{-} is H-bonded), considerably more so than UQ^{-} in the Q_A site in PBRCs.

Vibrational spectroscopic studies of quinones in the Q_A binding site are more advanced than corresponding studies of quinones in the A_1 binding site. There are several reasons for this: Firstly, (Q_A^{-}–Q_A) FTIR DS have been produced using photo-accumulation techniques. Photo-accumulation techniques can achieve higher sensitivity, and are considerably simpler to implement than TR techniques. Secondly, quinone incorporation into the Q_A binding site in PBRCs is straightforward, and thirdly specifically ^{13}C isotope labeled UQs have been incorporated

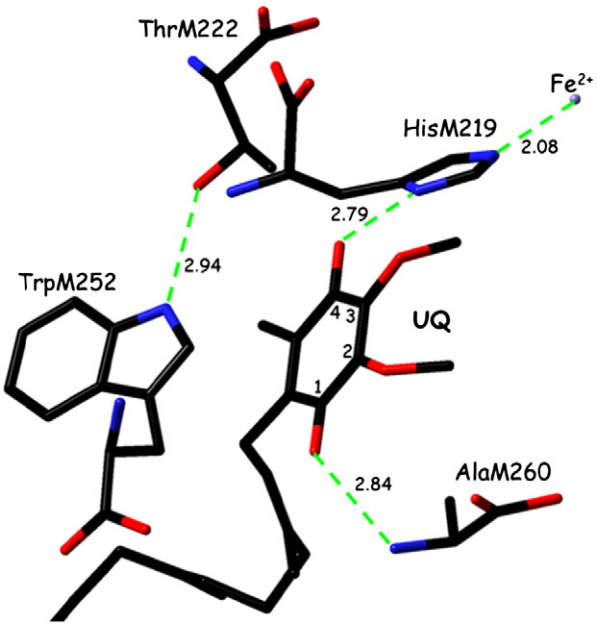

Fig. 10. View of UQ in the Q_A binding site in PBRCs from *Rb. sphaeroides*. Possible H-bonding interactions of the UQ carbonyl groups with the protein are shown (*dotted*). Figure was generated using PDB file 1PCR [71]. Nitrogen/oxygen/carbon atoms are blue/red/black, respectively.

into the Q_A binding site, and isotope edited FTIR DS have been produced [62,63]. This specific ^{13}C isotope labeling (carbon atoms 1–4 of UQ have been specifically ^{13}C labeled and incorporated) allows one to clearly discriminate protein bands from pigment bands in (Q_A^-–Q_A) FTIR DS. $^{13}C_4$ labeled 2MNQ has been incorporated into the A_1 binding site in PSI and studied using EPR spectroscopy [57]. Corresponding FTIR DS studies have not been published as of yet, although see reference [56] for a preliminary study.

(Q_A^-–Q_A) FTIR DS have been obtained for PBRCs with specific isotope labeled quinones incorporated [62,63], and the constructed isotope edited FTIR DS displays features (bands) that are associated only with the quinone in the binding site. For neutral UQ in the Q_A binding site, bands at 1660, 1628 and 1601 cm^{-1} were assigned to the C_1═O, C_2═C_3 and C_4═O groups, respectively [62,63]. The C_1═O group vibrational frequency is similar to that found for non-H-bonded UQ in solution, whereas the C_4═O vibrational frequency is downshifted ~59 cm^{-1}. From these results it was concluded that the C_1═O/C_4═O group of neutral UQ in the Q_A binding site is very weakly/very strongly H-bonded, respectively [62,63]. These conclusions are not supported by crystal structural data (Fig. 10) and other types of EPR and FTIR data [64–66], however.

To address this issue ONIOM type QM/MM calculations aimed at modeling the experimental isotope edited (Q_A^-–Q_A) FTIR DS were undertaken. Calculations were only undertaken for the neutral state of UQ in the Q_A binding site [64]. The ONIOM calculated spectra agree well with the experimental spectra. However, the calculations indicated that a very strongly H-bonded C_4═O group of UQ in the Q_A binding site is not required in order to explain the experimental spectra. The UQ in the Q_A binding site is still calculated to be asymmetrically H-bonded, but the C_4═O group is downshifted ~32 cm^{-1}, and not ~59 cm^{-1}, because of H-bonding.

It is worth noting that even with the large amount of experimental FTIR data available, it appears that it was still difficult to unambiguously interpret the experimental spectra, and it was only through a combination of experiment and computation that the above issue was adequately resolved.

To help confirm the validity of the QM/MM vibrational frequency calculations that were undertaken [64], further similar QM/MM calculations were undertaken for the neutral state of several different quinones incorporated into the Q_A binding site and, again, the calculated isotope edited FTIR DS were found to agree well with experimental spectra [67]. In all of the experimental spectra, and in the QM/MM calculated spectra, two separate bands due to the neutral quinone C═O modes were well resolved. This band separation being mainly a result of differences in H-bonding to each C═O group.

Sufficiently sensitive TR FTIR DS has not been undertaken using PSI particles with specifically $^{13}C_1$ and $^{13}C_4$ labeled PhQ (or 2MNQ) incorporated into the A_1 binding site (see reference [56], however), and the location of the bands associated with the C═O modes of the neutral quinone in the A_1 binding site have not been established with certainty. From the data discussed in this article it is clear that a band at ~1654 cm^{-1} is due to a C═O mode of neutral PhQ in the A_1 binding site (Table 1). It was suggested above that another C═O mode of neutral PhQ could give rise to a feature at ~1633 cm^{-1}. If this hypothesis is appropriate then the separation of the two C═O modes of PhQ in the A_1 binding site is 21 cm^{-1}, which is somewhat less than that found for UQ in the Q_A binding site (32 cm^{-1}). This suggests that the asymmetric H-bonding environment may be somewhat greater for neutral UQ in the Q_A binding site. This suggestion is only for the neutral quinone, but it is noted that it is at odds with conclusions derived from EPR studies of the quinone anion radicals in the A_1 and Q_A binding sites (see below) [57]. Of course, the suggested band assignments for the C═O groups of neutral PhQ in the A_1 binding site have not been tested/verified by ONIOM-type QM/MM vibrational frequency calculations, as has been done for UQ in the Q_A binding site. Clearly, more experimental data (specific isotope labeling of incorporated quinones), in combination with computational work, are required to establish band assignments unambiguously.

As mentioned above, experimental (Q_A^-–Q_A) isotope edited FTIR DS have been obtained by two groups [62,63]. Both groups incorporated specifically $^{13}C_1$ and $^{13}C_4$ labeled UQ into the Q_A binding site, and both obtained very similar isotope edited FTIR DS. For data in the anion spectral region (1500–1400 cm^{-1}), one group proposed that their data suggested that the two $C{=}O$ modes of UQ^- are coupled, and that the coupled $C{=}O$ mode is also coupled to $C{=}C$ modes [62]. The other group suggested that the $C{=}O$ modes of UQ^- are mainly uncoupled, with the C_4—O and C_1—O groups giving rise to bands at 1486 and 1466 cm^{-1}, respectively. In this latter case a distinct H-bond asymmetry that is typical for neutral UQ is preserved for UQ^-. This difference in hypothesis between the two groups has not been resolved.

In principle, QM/MM calculations could help address this issue. However, calculations for UQ^- in the Q_A binding site are more complicated than for the neutral state, partly because of spectral congestion in the anion spectral region, and partly because of a greater degree of mixing of the two UQ $C{=}O$ and $C{=}C$ modes. Isotope induced changes in the degree of mode mixing, in addition to isotope induced frequency shifts in an already congested spectral region, leads to calculated isotope edited DS that are complex, and that are difficult to compare to experimental spectra simply by visual inspection (G. Hastings, unpublished data). Because of these difficulties ONIOM type QM/MM calculated isotope edited difference spectra associated with UQ^- in the Q_A binding site have yet to be presented. So the extent of asymmetric H-bonding for UQ^- in the Q_A binding site is still an open question, at least in terms of analysis by FTIR DS.

As outlined above, for PhQ^- in the A_1 binding site there is no doubt that a $C{=}O$ mode gives rise to a band at 1495 cm^{-1}, while a mixed mode (with some $C{=}O$ character) gives rise to a band at 1415 cm^{-1}. In contrast, for PhQ^- incorporated into the Q_A binding site in PBRCs, a single $C{=}O$ mode is found at ~1444 cm^{-1}, while a predominantly $C{=}C$ mode is found at 1478 cm^{-1} [68]. This comparison suggests that the binding of PhQ^- in the Q_A and A_1 binding sites is very different. No QM/MM vibrational frequency calculations have been undertaken for PhQ^- in either the Q_A or A_1 binding sites, so questions on the nature of semiquinone binding in the Q_A or A_1 binding site are open, at least from the standpoint of vibrational spectroscopy. Specific hypotheses have

been proposed from EPR spectroscopic studies, however [57]. How or whether the hypotheses proposed from EPR studies are compatible with FTIR DS studies is, again, an open question.

6. Vibrational spectroscopy for assessing cofactor function

One commonly asked question is how knowledge of vibrational frequencies associated with molecular groups of bound quinones can be related to cofactor function. For the most part this question is essentially about how the observed spectroscopic data can be used to infer the redox potential of the quinone of interest in the binding site.

Parameters (band assignments) derived from FTIR DS measurements relate to the electronic structure of the cofactor in both the neutral and reduced states, which in turn can be used to determine redox properties. That is, to relate spectroscopic parameters to cofactor function, one approach is to assess how calculated spectroscopic parameters for particular molecular models relate to the experimental data. If the calculated vibrational frequencies for the neutral and reduced states for a particular molecular model compare well to experiment, then the constructed molecular model could be viewed as appropriate or useful, and it can then be used to calculate other parameters, such as single point energies and electron affinities, which directly relate to redox potential.

So far, for PhQ and PhQ^{-} (and other quinones) in the A_1 binding site, the vibrational frequencies of the molecular groups are just becoming available, and detailed vibrational frequency calculations to test hypothesis based on the experimental data are only just beginning. Given this dearth of knowledge, it is not surprising that little has been published so far concerning the redox properties of quinones in the A_1 binding site, as can be inferred from vibrational spectroscopic data.

7. Summary

The experimental work that has been undertaken, as described in this review, indicates that TRSS FTIR DS studies of quinones in the A_1 binding site are still in their infancy, with a range of experiments possible for different quinones (including isotope labeled versions) incorporated into the A_1 binding site. In addition, ONIOM-type QM/MM vibrational frequency calculations for quinones in the A_1 binding site are only just beginning, and no work has been published in this area as of yet. Part of the problem for development of these computational methods is that the experimental data needed to assess the calculations is not available, or it is only just becoming available. Thus there are many opportunities in both the experimental and computational realms for vibrational spectroscopic studies of quinones in the A_1 binding site in PSI.

Acknowledgments

Some of the recent work outlined in this manuscript was supported by the Qatar National Research Fund, grant 4-183-1-034. Older work was supported by the National Research Initiative of the United States Department of Agriculture Cooperative State Research Education and Extension Service (2004-35318-14889). Much of the recent time resolved step scan FTIR spectroscopy work, as well as much of the computational work, was undertaken by Nan Zhao. All of the visible time resolved spectroscopy work was undertaken by Hiroki Makita. Nan and Hiroki are currently graduate students in my research group. I would also like to acknowledge all previous students who have worked with me in this area, in particular Velautham Sivakumar, Priyangi Bandaranayake, Ruili Wang and Sreeja Parameswaran.

References

[1] G. Hastings, FTIR studies of the intermediate electron acceptor A_1, in: J. Golbeck (Ed.), Photosystem I: The Light Driven Plastocyanin:Ferredoxin Oxidoreductase, Springer, Dordrecht, 2006, pp. 301–318.
[2] D. Walker, Energy, plants and man, 2nd ed. Oxygraphics, Brighton, East Sussex: Mill Valley, CA, 1993.
[3] J. Barber, The Photosystems: Structure, Function, and Molecular Biology, Elsevier Science Publishers, Amsterdam, New York, 1992.
[4] B. Ke, Photosynthesis: Photobiochemistry and Photobiophysics, Kluwer Academic Publishers, Dordrecht; Boston, 2001.
[5] J. Golbeck, Photosystem I the Light Driven Plastocyanin:Ferridoxin Oxidoreductase, Springer, Dordrecht, 2006.
[6] P. Chitnis, Q. Xu, V. Chirnis, R. Nechustai, Function and Organization of Photosystem I Polypeptides, Photosynth. Res. 44 (1995) 23–40.
[7] J. Golbeck, Photosystem I in Cyanobacteria, in: D. Bryant (Ed.), Advances in Photosynthesis. Molecular Biology of Cyanobacteria, Kluwer Academic Publishers, 1995, pp. 311–360.
[8] H. Pakrasi, Genetic Analysis of the Form and Function of Photosystem I and Photosystem-II, Annu. Rev. Genet., vol. 29, 1995, pp. 755–756.
[9] J.H. Golbeck, D. Bryant, Photosystem I, Current topics in bioenergetics, vol. 16, Academic Press, New York, 1991, pp. 83–175.
[10] P. Fromme, I. Grotjohann, Structural analysis of cyanobacterial photosystem I, in: J.H. Golbeck (Ed.), Photosystem I: The Light Driven Plastocyanin:Ferredoxin Oxidoreductase, vol. 24, Springer, Dordrecht, 2006, pp. 47–69.
[11] B. Ke, The primary electron donor of photosystem I-P700, Photosynthesis: Photobiochemistry and Photobiophysics, Kluwer Academic Publishers, Dordrecht; Boston, 2001, pp. 463–477.
[12] P. Jordan, P. Fromme, H.T. Witt, O. Klukas, W. Saenger, N. Krauss, Three-dimensional structure of cyanobacterial photosystem I at 2.5 angstrom resolution, Nature 411 (2001) 909–917.
[13] B. Ke, The primary electron acceptor A_0 of photosystem I, Photosynthesis: Photobiochemistry and Photobiophysics, Kluwer Academic Publishers, Dordrecht; Boston, 2001, pp. 555–578.
[14] B. Ke, The iron–sulfur center FeS-X of photosystem I, the photosystem I core complex, and interaction of the FeS-X domain with FeS-A. FeS-B, Photosynthesis: Photobiochemistry and Photobiophysics, Kluwer Academic Publishers, Dordrecht; Boston, 2001, pp. 527–554.
[15] B. Ke, P430: the spectral species representing the terminal electron acceptor in photosystem I, Photosynthesis: Photobiochemistry and Photobiophysics, Kluwer Academic Publishers, Dordrecht; Boston, 2001, pp. 505–526.
[16] S. Savikhin, Ultrafast optical spectroscopy of photosystem I, in: J. Golbeck (Ed.), Photosystem I The Light-Driven Plastocyanin: Ferredoxin Oxidoreductase, Springer, Dordrecht, 2006, pp. 155–175.
[17] G. Hastings, S. Hoshina, A.N. Webber, R.E. Blankenship, Universality of energy and electron-transfer processes in photosystem-I, Biochemistry 34 (1995) 15512–15522.
[18] E. Schlodder, K. Falkenberg, M. Gergeleit, K. Brettel, Temperature dependence of forward and reverse electron transfer from A_1^-, the reduced secondary electron acceptor in photosystem I, Biochemistry 37 (1998) 9466–9476.
[19] K. Redding, A. van der Est, The directionality of electron transfer in photosystem I, in: J.H. Golbeck (Ed.), Photosystem I: The Light Driven Plastocyanin:Ferredoxin Oxidoreductase, vol. 24, Springer, Dordrecht, 2006, pp. 413–437.
[20] F. Rappaport, B. Diner, K. Redding, Optical measurements of secondary electron transfer in photosystem I, in: J.H. Golbeck (Ed.), Photosystem I: The Light Driven Plastocyanin:Ferredoxin Oxidoreductase, vol. 24, Springer, Dordrecht, 2006, pp. 223–244.
[21] N. Srinivasan, J.H. Golbeck, Protein-cofactor interactions in bioenergetic complexes: the role of the A(1A) and A(1B) phylloquinones in Photosystem I, Biochim. Biophys. Acta Bioenerg. 1787 (2009) 1057–1088.
[22] S. Santabarbara, P. Heathcote, M.C.W. Evans, Modelling of the electron transfer reactions in Photosystem I by electron tunnelling theory: the phylloquinones bound to the PsaA and the PsaB reaction centre subunits of PSI are almost isoenergetic to the iron–sulfur cluster Fx, Biochim. Biophys. Acta Bioenerg. 1708 (2005) 283–310.
[23] E. Nabedryk, Light-induced Fourier transform infrared difference spectroscopy of the primary electron donor in photosynthetic reaction centers, in: H.H. Mantsch, D. Chapman (Eds.), Infrared spectroscopy of biomolecules, Wiley-Liss, New York, 1996, pp. 39–81.
[24] W. Mäntele, Infrared vibrational spectroscopy of photosynthetic reaction centers, in: J. Deisenhofer, J. Norris (Eds.), The Photosynthetic reaction center, vol. 2, Academic Press, San Diego, 1993, pp. 239–283.
[25] W. Mäntele, Infrared vibrational spectroscopy of reaction centers, in: R.E. Blankenship, M.T. Madigan, C.E. Bauer (Eds.), Anoxygenic Photosynthetic Bacteria, Kluwer Academic Publishers, Dordrecht; Boston, 1995, pp. 627–647.
[26] J. Breton, Fourier transform infrared spectroscopy of primary electron donors in type I photosynthetic reaction centers, Biochim. Biophys. Acta 1507 (2001) 180–193.
[27] J. Breton, FTIR studies of the primary electron donor, P700, in: J. Golbeck (Ed.), Photosystem I: The Light Driven Plastocyanin:Ferredoxin Oxidoreductase, Springer, Dordrecht, 2006, pp. 271–289.
[28] W. Uhmann, A. Becker, C. Taran, F. Siebert, Time-resolved FT-IR absorption spectroscopy using a step-scan interferometer, Appl. Spectrosc. 45 (1991) 390–397.
[29] G. Hastings, Time-resolved step-scan Fourier transform infrared and visible absorption difference spectroscopy for the study of photosystem I, Appl. Spectrosc. 55 (2001) 894–900.
[30] S.E. Plunkett, J.L. Chao, T.J. Tague, R.A. Palmer, Time-resolved step-scan FT-IR spectroscopy of the photodynamics of carbonmonoxymyoglobin, Appl. Spectrosc. 49 (1995) 702–708.
[31] X. Hu, H. Frei, T.G. Spiro, Nanosecond step-scan FTIR spectroscopy of hemoglobin: ligand recombination and protein conformational changes, Biochemistry 35 (1996) 13001–13005.

[32] C. Kotting, J. Guldenhaupt, K. Gerwert, Time-resolved FTIR spectroscopy for monitoring protein dynamics exemplified by functional studies of Ras protein bound to a lipid bilayer, Chem. Phys. 396 (2012) 72–83.
[33] G. Hastings, V.M. Ramesh, R. Wang, V. Sivakumar, A. Webber, Primary donor photo-oxidation in photosystem I: a re-evaluation of ($P700^+$–P700) Fourier transform infrared difference spectra, Biochemistry 40 (2001) 12943–12949.
[34] J. Breton, E. Nabedryk, W. Leibl, FTIR study of the primary electron donor of photosystem I (P700) revealing delocalization of the charge in P700(+) and localization of the triplet character in (3)P700, Biochemistry 38 (1999) 11585–11592.
[35] S. Parameswaran, R. Wang, G. Hastings, Calculation of the vibrational properties of chlorophyll a in solution, J. Phys. Chem. B 112 (2008) 14056–14062.
[36] G. Hastings, R. Wang, Vibrational mode frequency calculations of chlorophyll-d for assessing (P740(+)–P740) FTIR difference spectra obtained using photosystem I particles from Acaryochloris marina, Photosynth. Res. 95 (2008) 55–62.
[37] R.L. Wang, S. Parameswaran, G. Hastings, Density functional theory based calculations of the vibrational properties of chlorophyll-a, Vib. Spectrosc. 44 (2007) 357–368.
[38] S.L. Bender, B.A. Barry, Light-induced dynamics in photosystem I electron transfer, Biophys. J. 95 (2008) 3927–3934.
[39] M. Di Donato, A.D. Stahl, I.H.M. van Stokkum, R. van Grondelle, M.-L. Groot, Cofactors involved in light-driven charge separation in photosystem I identified by subpicosecond infrared spectroscopy, Biochemistry 50 (2010) 480–490.
[40] T.W. Johnson, G. Shen, B. Zybailov, D. Kolling, R. Reategui, S. Beauparlant, I.R. Vassiliev, D.A. Bryant, A.D. Jones, J.H. Golbeck, P.R. Chitnis, Recruitment of a foreign quinone into the A_1 site of photosystem I. I. Genetic and physiological characterization of phylloquinone biosynthetic pathway mutants in Synechocystis sp. pcc 6803, J. Biol. Chem. 275 (2000) 8523–8530.
[41] B. Zybailov, A. van der Est, S.G. Zech, C. Teutloff, T.W. Johnson, G. Shen, R. Bittl, D. Stehlik, P.R. Chitnis, J.H. Golbeck, Recruitment of a foreign quinone into the A(1) site of photosystem I. II. Structural and functional characterization of phylloquinone biosynthetic pathway mutants by electron paramagnetic resonance and electron–nuclear double resonance spectroscopy, J. Biol. Chem. 275 (2000) 8531–8539.
[42] A.Y. Semenov, I.R. Vassiliev, A. van Der Est, M.D. Mamedov, B. Zybailov, G. Shen, D. Stehlik, B.A. Diner, P.R. Chitnis, J.H. Golbeck, Recruitment of a foreign quinone into the A_1 site of photosystem I. Altered kinetics of electron transfer in phylloquinone biosynthetic pathway mutants studied by time-resolved optical, EPR, and electrometric techniques, J. Biol. Chem. 275 (2000) 23429–23438.
[43] K.M. Bandaranayake, R. Wang, T.W. Johnson, G. Hastings, Time-resolved FTIR difference spectroscopy for the study of photosystem I particles with plastoquinone-9 occupying the A1 binding site, Biochemistry 45 (2006) 12733–12740.
[44] B. Zybailov, Modified Quinone Acceptors In Photosystem I, Biochemistry, Microbiology, and Molecular Biology, The Pennsylvania State University, 2003.
[45] Y.N. Pushkar, O. Ayzatulin, D. Stehlik, Transient and pulsed EPR study of O-17-substituted methyl-naphthoquinone as radical anion in the A(1) binding site of photosystem I and in frozen solution, Appl. Magn. Reson. 28 (2005) 195–211.
[46] K. Bandaranayake, R. Wang, G. Hastings, Modification of the phylloquinone in the A_1 binding site in photosystem I studied using time-resolved FTIR difference spectroscopy and density functional theory, Biochemistry 45 (2006) 4121–4127.
[47] V. Sivakumar, R. Wang, G. Hastings, A(1) reduction in intact cyanobacterial photosystem I particles studied by time-resolved step-scan Fourier transform infrared difference spectroscopy and isotope labeling, Biochemistry 44 (2005) 1880–1893.
[48] R. Wang, G. Hastings, Computed infrared spectra of protonated and metal-bound 4-methylimidazole, in: A. van der Est, D. Bruce (Eds.), Photosynthesis: Fundamental Aspects to Global Perspectives. Procedings of the 13th International Conference In Photosynthesis, Alliance Communications Group, Lawrence, KS, 2005, pp. 70–71.
[49] R. Wang, V. Sivakumar, T.W. Johnson, G. Hastings, FTIR difference spectroscopy in combination with isotope labeling for identification of the carbonyl modes of P700 and P700+ in photosystem I, Biophys. J. 86 (2004) 1061–1073.
[50] K. Bandaranayake, V. Sivakumar, R. Wang, G. Hastings, Modeling the A_1 binding site in photosystem I. Density functional theory for the calculation of "anion–neutral" FTIR difference spectra of phylloquinone, Vib. Spectrosc. 42 (2006) 78–87.
[51] G. Hastings, K.M.P. Bandaranayake, E. Carrion, Time-resolved FTIR difference spectroscopy in combination with specific isotope labeling for the study of A(1), the secondary electron acceptor in photosystem 1, Biophys. J. 94 (2008) 4383–4392.
[52] T.W. Johnson, S. Naithani, C. Stewart, B. Zybailov, A.D. Jones, J.H. Golbeck, P.R. Chitnis, The menD and menE homologs code for 2-succinyl-6-hydroxyl-2, 4-cyclohexadiene-1-carboxylate synthase and O-succinylbenzoic acid-CoA synthase in the phylloquinone biosynthetic pathway of Synechocystis sp PCC 6803, Biochim. Biophys. Acta 1557 (2003) 67–76.
[53] T.W. Johnson, B. Zybailov, A.D. Jones, R. Bittl, S. Zech, D. Stehlik, J.H. Golbeck, P.R. Chitnis, Recruitment of a foreign quinone into the A_1 site of photosystem I. In vivo replacement of plastoquinone-9 by media-supplemented naphthoquinones in phylloquinone biosynthetic pathway mutants of *Synechocystis* sp. PCC 6803, J. Biol. Chem. 276 (2001) 39512–39521.
[54] Y. Sakuragi, B. Zybailov, G.Z. Shen, A.D. Jones, P.R. Chitnis, A. van der Est, R. Bittl, S. Zech, D. Stehlik, J.H. Golbeck, D.A. Bryant, Insertional inactivation of the menG gene, encoding 2-phytyl-1,4-naphthoquinone methyltransferase of Synechocystis sp PCC 6803, results in the incorporation of 2-phytyl-1,4-naphthoquinone into the A(1) site and alteration of the equilibrium constant between A(1) and F-x in photosystem I, Biochemistry 41 (2002) 394–405.
[55] Y.S. Sakuragi, D.A. Bryant, Genetic manipulation of quinone biosynthesis in cyanobacteria, in: J.H. Golbeck (Ed.), Photosystem I: The Light Driven Plastocyanin:Ferredoxin Oxidoreductase, Springer, Dordrecht, 2006, pp. 205–222.
[56] G. Hastings, K.M.P. Bandaranayake, Quinone anion bands in A_1^-/A_1 FTIR difference spectra investigated using photosystem I particles with specifically labeled naphthoquinones incorporated into the A_1 binding site, in: J. Allen, E. Gantt, J. Golbeck, B. Osmond (Eds.), Photosynthesis. Energy from the Sun. 14th International Congress on Photosynthesis Research 2007, Springer, 2008, pp. 69–72, (Chapter 12).
[57] Y.N. Pushkar, J.H. Golbeck, D. Stehlik, H. Zimmermann, Asymmetric hydrogen-bonding of the quinone cofactor in photosystem I probed by C-13-labeled naphthoquinones, J. Phys. Chem. B 108 (2004) 9439–9448.
[58] S. Mula, A. Savitsky, K. Mobius, W. Lubitz, J.H. Golbeck, M.D. Mamedov, A.Y. Semenov, A.V. der Est, Incorporation of a high potential quinone reveals that electron transfer in photosystem I becomes highly asymmetric at low temperature, Photochem. Photobiol. Sci. 11 (2012) 946–956.
[59] V.P. Shinkarev, B. Zybailov, I.R. Vassiliev, J.H. Golbeck, Modeling of the $P700^+$ charge recombination kinetics with phylloquinone and plastoquinone-9 in the A_1 site of photosystem I, Biophys. J. 83 (2002) 2885–2897.
[60] R. Agalarov, K. Brettel, Temperature dependence of biphasic forward electron transfer from the phylloquinone(s) A1 in photosystem I: only the slower phase is activated, Biochim. Biophys. Acta 1604 (2003) 7–12.
[61] J.A. Bautista, F. Rappaport, M. Guergova-Kuras, R.O. Cohen, J.H. Golbeck, J.Y. Wang, D. Beal, B.A. Diner, Biochemical and biophysical characterization of photosystem I from phytoene desaturase and xi-carotene desaturase deletion mutants of Synechocystis sp PCC 6803, J. Biol. Chem. 280 (2005) 20030–20041.
[62] J. Breton, C. Boullais, J.R. Burie, E. Nabedryk, C. Mioskowski, Binding sites of quinones in photosynthetic bacterial reaction centers investigated by light-induced FTIR difference spectroscopy: assignment of the interactions of each carbonyl of Q_A in *Rhodobacter sphaeroides* using site-specific ^{13}C-labeled ubiquinone, Biochemistry 33 (1994) 14378–14386.
[63] R. Brudler, H.J. de Groot, W.B. van Liemt, W.F. Steggerda, R. Esmeijer, P. Gast, A.J. Hoff, J. Lugtenburg, K. Gerwert, Asymmetric binding of the 1- and 4-C═O groups of QA in Rhodobacter sphaeroides R26 reaction centres monitored by Fourier transform infra-red spectroscopy using site-specific isotopically labelled ubiquinone-10, EMBO J. 13 (1994) 5523–5530.
[64] H.P. Lamichhane, G. Hastings, Calculated vibrational properties of pigments in protein binding sites, Proc. Natl. Acad. Sci. U. S. A. 108 (2011) 10526–10531.
[65] C.A. Wraight, M.R. Gunner, The acceptor quinones of purple photosynthetic bacteria—structure and spectroscopy, in: C. Hunter, F. Daldal, T. MC, B. TJ (Eds.), The Purple Phototrophic Bacteria, Springer, 2009, pp. 379–405.
[66] J. Breton, J. Lavergne, M.C. Wakeham, E. Nabedryk, M.R. Jones, The unusually strong hydrogen bond between the carbonyl of Q(A) and his M219 in the Rhodobacter sphaeroides reaction center is not essential for efficient electron transfer from Q(A)(−) to Q(B), Biochemistry 46 (2007) 6468–6476.
[67] N. Zhao, H.P. Lamichanne, G. Hastings, Comparison of calculated and experimental isotope edited FTIR difference spectra for purple bacterial photosynthetic reaction centers with different quinones incorporated into the QA binding site, Front. Plant Sci. 4 (2013).
[68] J. Breton, J.R. Burie, C. Berthomieu, G. Berger, E. Nabedryk, The binding sites of quinones in photosynthetic bacterial reaction centers investigated by light-induced FTIR difference spectroscopy: assignment of the Q_A vibrations in *Rhodobacter sphaeroides* using ^{18}O- or ^{13}C-labeled ubiquinone and vitamin K_1, Biochemistry 33 (1994) 4953–4965.
[69] V. Sivakumar, R. Wang, T. Johnson, G. Hastings, A_1 reduction in intact cyanobacterial photosystem I studied using time-resolved step-scan Fourier transform infra-red difference spectroscopy in combination with site directed mutagenesis and quinone exchange experiments, in: A. van der Est, D. Bruce (Eds.), Photosynthesis: Fundamental Aspects to Global Perspectives, Alliance Communications Group, Lawrence, KS, 2005, pp. 59–60.
[70] K. Brettel, Electron transfer and arrangement of the redox cofactors in photosystem I, Biochim. Biophys. Acta 1318 (1997) 322–373.
[71] M.H. Stowell, T.M. McPhillips, D.C. Rees, S.M. Soltis, E. Abresch, G. Feher, Light-induced structural changes in photosynthetic reaction center: implications for mechanism of electron–proton transfer, Science 276 (1997) 812–816.